# SUPERHUMPS IN CATACLYSMIC BINARIES.

# XVIII. IY URSAE MAJORIS

JOSEPH PATTERSON,[1] JONATHAN KEMP,[1,2] LASSE JENSEN,[3] TONNY VANMUNSTER,[4]

DAVID R. SKILLMAN,[5] BRIAN MARTIN,[6] ROBERT FRIED,[7] AND JOHN R. THORSTENSEN[8]

submitted • *Publications of the Astronomical Society of the Pacific* • 2000 April 7

2000 August 29 Revision

[1] Department of Astronomy, Columbia University, 550 West 120th Street, New York, NY 10027; jop@astro.columbia.edu

[2] Currently at: Joint Astronomy Centre, University Park, 660 North A`ohōkū Place, Hilo, HI 96720; j.kemp@jach.hawaii.edu

[3] Center for Backyard Astrophysics (Denmark), Søndervej 38, DK–8350 Hundslund, Denmark; teist@image.dk

[4] Center for Backyard Astrophysics (Belgium), Walhostraat 1A, B–3401 Landen, Belgium; tonny.vanmunster@advalvas.be

[5] Center for Backyard Astrophysics (East), 9517 Washington Avenue, Laurel, MD 20723; dskillman@home.com

[6] Center for Backyard Astrophysics (Alberta), Department of Physics, King's University College, 9125 50th Street, Edmonton, AB T5H 2M1; bmartin@kingsu.ab.ca

[7] Braeside Observatory, Post Office Box 906, Flagstaff, AZ 86002; captain@braeside.org

[8] Department of Physics and Astronomy, Dartmouth College, 6127 Wilder Laboratory, Hanover, NH 03755; thorstensen@dartmouth.edu

## ABSTRACT

We report photometric and spectroscopic observations of the eclipsing dwarf nova IY Ursae Majoris (= Takamizawa V85). During its January 2000 superoutburst, the star flashed superhumps with a period of 0.07583 d, 2.6% longer than the true orbital period. These waves rumbled through the light curve for ~20 days. They appeared compatible with their common interpretation as the lower precessional sideband of the orbital clock: at a frequency $\omega_o - \Omega$, where $\omega_o$ is the orbital frequency and $\Omega$ is the accretion disk's assumed precessional frequency. But the power spectrum of the superhumps showed additional complexity, including signals at $3\omega_o - \Omega$, $4\omega_o - \Omega$, and $5\omega_o - \Omega$. The latter probably arise from gravitational perturbation of more complex but still resonant (e.g., spiral) structures in the disk.

During eruption, the light curve across eclipse showed a large, bright accretion disk. Timings of minima and eclipse contacts reveal that the disk was quite eccentric, with $e$=0.29±0.06, and that this eccentric shape moved around with the putative precession period of 2.9 d. As the eruption faded, the eclipses began to reveal the signature of the white dwarf and the hot spot at the disk's edge. "Late" superhumps raged at high amplitude for another ~10 days, although the disk had seemingly contracted by ~30%. Spectroscopy in quiescence showed strong doubled emission lines, typical of low-$\dot{M}$ dwarf novae, and an $S$-wave with a semiamplitude of 750 km/s.

The travelling knife-edge of the secondary's limb made it possible to separate all the important light sources in quiescence: white dwarf, secondary star, hot spot, accretion disk. The ingress and egress phases of the white-dwarf eclipse were very brief, declining from ~40 s to 25 s. The brightness of the white dwarf also varied, rapidly at first and then slowly. Eclipse measurements in quiescence lead to estimates for the fundamental parameters of the binary: $q$=0.13±0.02, $M_2$=0.12±0.02 $M_\odot$, $M_1$=0.86±0.11 $M_\odot$, $i$=86.8±1.5°. We estimate a distance of 190±60 pc. With a small distance, a high inclination, vigorous superhumps, bright emission lines, and clear lines of sight to the central object, IY UMa furnishes a promising new laboratory for studying accretion-disk physics.


*Subject headings*: accretion, accretion disks — binaries: close — novae, cataclysmic variables — stars: individual (IY Ursae Majoris)

## 1. INTRODUCTION

Among cataclysmic variables, and among binary stars in general, eclipses supply a powerful diagnostic tool. Eclipses provide a precise timing signature in the orbital motion, enabling measurement of small period and phase changes, sizes of different components in the binary, and the relative contributions of different components to the total light. Techniques for extracting this information were pioneered by Russell and Shapley (1912), and have been responsible for nearly everything we know about stellar masses and radii. During the 1970s, fast photometry of eclipsing cataclysmic variables (CVs) showed well-defined discrete structures during eclipse, and their study has also been very rewarding. A host of important papers on eclipse analysis (e.g., Ritter & Schroeder 1979, Wood et al. 1986, Wood et al. 1989) has made this the source of some of the most reliable measurements we have on CVs.

Of all eclipsing CVs, the most interesting are the dwarf novae, since the changing eclipse shapes give clear evidence of the dramatic disk changes between outburst and quiescence. The general pattern was first found in Z Cha by Warner (1974): a broad smooth eclipse in eruption signified a large luminous accretion disk, while the quiescent eclipse showed small structures identifiable as the white dwarf and the bright spot at the disk edge. Many subsequent studies of Z Cha (Wood et al. 1986, O'Donoghue 1986, Robinson et al. 1995) have exploited the rich diagnostic power of eclipses to measure the fundamental parameters of the binary. Similar analyses have been carried out for HT Cas (Patterson 1981, Horne et al. 1992) and OY Car (Wood et al. 1989).

The report of superhumps and eclipses in IY UMa (see Uemura et al. 2000 for its brief history) launched our photometric and spectroscopic campaign on this newly discovered dwarf nova. In this paper we report the results. The superhumps were found to be essentially the *common superhumps* found in all SU UMa-type dwarf novae, although their high harmonics showed a complexity rarely found (not previously certified in any dwarf nova). These evolved into *late* superhumps, which continued long after the star faded back towards quiescence. Eclipse measurements appear to confirm the presence of a precessing elliptical disk during and just after superoutburst. They also constrain the binary parameters fairly well, yielding $q$=0.13±0.02, $M_2$=0.12±0.02 $M_\odot$, $M_1$=0.86±0.11 $M_\odot$, and $i$=86.8±1.5°. Further observations are likely to redeem the star's promise as an excellent new laboratory for studying accretion-disk astrophysics.

## 2. PHOTOMETRY

IY UMa was the 85th object discovered in a photographic survey for new variable stars by Kesao Takamizawa (hence its preliminary name, Tmz V85). Takamizawa discovered the star in outburst at $m_{pg}$=13.6 on 9 Nov 1997. Aside from this solitary point, all other visual and photographic observations were merely upper limits (typically $m_{pg}$>15) until January 2000, when the new outburst was reported (Schmeer 2000). After receiving this report, we began time-series photometry on 19 January, and continued for 17 nights with only a few gaps in coverage. To this was added a few scattered observations obtained over the next 70 d, to study long-term trends. Most observations were obtained in *V* light with the 1.3 m reflector of MDM Observatory, with

many other time series provided by several telescopes in the Center for Backyard Astrophysics network (CBA, Skillman & Patterson 1993). This wide range of terrestrial longitude, from Denmark to western Canada, proved critical in overcoming potential 24-hour aliases in the period structure. All photometry was done differentially with respect to GSC 3829–910, a nearby (2' SW from the variable) comparison star with $V$=13.56 and $B–V$=0.92. Although most CBA telescopes operate in unfiltered light, we obtained some *V*-band and/or *BVRI* coverage simultaneous with each contributing telescope, which enabled us to transform all the photometry to *V* magnitudes. The uncertainty in this transformation is ~0.07 mag; the random error varies from 0.01 mag in the MDM light curves to ~0.03–0.06 mag in the small-telescope light curves.

The complete log of photometry is given in Table 1. The rightmost column gives the *V* magnitude averaged over the night, or two measurements for nights with a severe trend. In Figure 1 we show the eruption light curve, by combining these data with other magnitudes (also transformed with simultaneous *V*-band measurement) from the IAU Circulars and the VSNET archive (`http://www.kusastro.kyoto-u.ac.jp/vsnet/`). The eruption looks like a garden-variety superoutburst of an SU Ursae Majoris-type dwarf nova: a rapid 4-magnitude rise, followed by a slow decline at 0.12 mag/day, a rapid fall at ~1 mag/day, and a final slow approach to quiescence. In the one serendipitous observation long before outburst (Henden 2000), the star was found to be at $V$=17.63 at orbital phase 0.57; from the light curves presented below, this suggests an orbital average around $V$=17.3 at that time. Thus the light curve of Figure 1 probably approaches true quiescence.[1]

We also obtained some snapshot and time-series photometry through *UBVRI* filters, and extensive time series through a Schott *BG38* filter transmitting over 3700–6000 Å (effectively "wide blue" for a blue spectral slope like that of a cataclysmic variable). Each type of measurement was strictly simultaneous with a *V* measurement (using the two telescopes of MDM Observatory); and we used this simultaneity, along with multicolor observation of nearby standards, to establish calibration. Calibration of the *BG38* filter (to within the 0.07 mag stated above) was particularly useful, as this wide filter has the high throughput needed for good-quality light curves at high time resolution.

IY UMa has a faint companion star 4" away to the NE, at 19th magnitude. Some CBA photometry included this star, but was not significantly affected since the dwarf nova was much brighter at that time. The nearby star became a nuisance when IY UMa dropped to $B$~20 at mid-eclipse in quiescence, but was excluded by the IRAF measuring routines as long as the images were adequately exposed. Special care was taken during eclipse to avoid this contamination.

In the following we shall frequently use a truncated version of Julian Date, with JD denoting "JD–2451500". We shall also refer to "day *x*" of the eruption, where $x$ = JD–2451556; we estimate the latter as the eruption's start, with an uncertainty of ±2 days.

## 3. SUPEROURBURST

[1] The $V$=18.4 measurement cited by Uemura et al. (2000) was taken in eclipse, hence does not represent true quiescence.

Figure 2 shows sample nightly light curves during superoutburst, with three segments spliced over 2-day intervals. These show all the essential features. Recurrent deep eclipses occur on a strict schedule, revealing the underlying 0.07391 d binary period. In addition a powerful wave rumbles through the light curve. Figure 2 shows that the wave drifts in orbital phase (i.e., relative to the eclipse), indicating that the period differs slightly from $P_{orb}$. Thus the wave is evidently a "superhump", a standard signature of SU UMa-type dwarf novae (Warner 1985).

The superhump amplitude changes significantly, mostly dependent on the difference between hump and eclipse phase. When it coincides with eclipse, the hump is more difficult to see (although manifest by the reduced eclipse depth). There are also *intrinsic* changes in the superhump. Note in particular the changes in waveform occurring during JD 66–70. A higher-frequency wiggle grows steadily through JD 66–68, and then disappears a day later. This — the ability to manufacture signals at higher frequency — is an interesting aspect of superhumps, deserving more attention.

After removing the deep eclipses, we calculated the power spectrum of the 8-night light curve from the discrete Fourier transform. The result, displayed in Figure 3, shows a strong signal at 13.18±0.01 c/d, the basic superhump frequency $\omega_s$. Three other significant signals are present, marked by arrows and labeled with their frequencies in c/d. Two are harmonics of the fundamental, merely indicating a nonsinusoidal waveform (see inset). The feature at 40.23 c/d is more interesting. In superhump terminology, $\omega_s$ is often written as $\omega_o$–$\Omega$, where $\omega_o$ is the orbital frequency and $\Omega$ is the presumed frequency of apsidal precession (in the standard theory of superhumps; Whitehurst 1988, Osaki 1989, Lubow 1991). In this case $\Omega$=0.35±0.02, so this feature is consistent with $3\omega_o$–$\Omega$.[2]

## 4. POST–SUPEROUTBURST

During JD 69–70 the star dropped rapidly to $V$=16.8, and the star began its slow final decline to quiescence. Time-series photometry continued throughout, with sample nightly light curves shown in Figure 4. A prominent wave continued to rumble through the light curve, although with very great amplitude excursions. Eclipses became deeper and narrower, with very sharp features — proving that during this interval most of the light came from quite small structures in the binary.

The upper panel of Figure 5 shows a 9-night light curve, with eclipses removed, just after

[2] Other fine structure near the harmonics is possibly present too. We attempted to isolate these components by "cleaning" (removing aliases of the stronger signals) the power spectrum; but this did not give reliable results. The reason is that the weaker signals appear to be somewhat transient, not enduring with near-constant amplitude through the 8 nights. This alters the alias pattern in an essentially unknowable way, preventing accurate removal. Under such circumstances, there is some danger that spectral cleaning can introduce artificial features into the power spectrum.

the end of superoutburst. Wave excursions to low amplitude are seen to occur at 3-day intervals, suggesting the possibility that these arise from the beating of signals closely spaced in frequency. The power spectrum of the middle panel of Figure 5 verifies this, revealing strong signals at 13.53 and 13.22 c/d — respectively $\omega_o$ and the slightly blue-shifted remnant of the superhump. Of the four other significant signals, also marked with arrows, two are merely harmonics of the orbital signal (27.05 and 40.61 at $2\omega_o$ and $3\omega_o$ respectively). The other two are more interesting, occurring at $4\omega_o$–0.29 and $5\omega_o$–0.30 c/d — consistent with identification as $4\omega_o$–$\Omega$ and $5\omega_o$–$\Omega$ in standard superhump terminology ($\Omega$ is the frequency difference between principal signals, and Figure 4 shows that it has shifted from 0.35 in the main superoutburst to 0.31 c/d in this later stage).

The lowest panel of Figure 5 shows the light curve folded at the orbital and superhump frequencies. The mean orbital light curve shows the usual features associated with eclipsing dwarf novae in quiescence, and is very similar to that of the well-studied binary OY Carinae (see Figure 2 of Wood et al. 1989). The superhump is seen to remain quite large, with a full amplitude of 0.5 mag. However, no observation after JD 78 showed a superhump, indicating that it faded below detection limits 8–13 days after the rapid decline.

## 5. ORIGIN OF STRUCTURE IN HARMONICS

Most superhumps in dwarf novae are fairly powerful signals which are somewhat non-sinusoidal. Therefore the expectation is that their power spectra should reveal simple harmonics of the fundamental frequency $\omega_s=\omega_o-\Omega$. And indeed, our experience from studying a few dozen of these stars is that this is correct: the fundamental dominates, with often a second signal at $2(\omega_o-\Omega)$, and occasionally higher harmonics, all simple multiples of $\omega_s$. Yet IY UMa shows much greater complexity, with signals at $3\omega_o$–$\Omega$, $4\omega_o$–$\Omega$, and $5\omega_o$–$\Omega$. Why should that be?

The reason is perhaps the same reason there are superhumps at all. A resonance in the disk triggers growth of an eccentric instability, and the disk assumes a complex shape. If that shape is stable and there is no precession, then the orbiting secondary tugs on the disk with frequencies $\omega_o$, $2\omega_o$, $3\omega_o$, $4\omega_o$, etc., depending on how complex are the deviations from a simple ellipse. Still assuming a stable shape but correcting for precession, all these frequencies will be red-shifted by $-\Omega$, as observed. Thus we could account for these signals in a conventional way (tidal stirring of the disk), if we hypothesize higher-order azimuthal structures in the disk that are resonant with $P_{orb}$. Many theoretical studies of disks with SPH simulations (e.g., Lubow 1991, Simpson & Wood 1998) have shown such structures, sometimes described as "spiral waves".

There are demerits to this hypothesis, however. Since it only produces $-\Omega$ sidebands, it does not explain the much richer harmonic structure in some permanent superhumpers (e.g., AM CVn, Skillman et al. 1999). And it does not explain in any convincing way (one can always mutter excuses about binary inclination) why these effects appear preferentially in IY UMa. So the hypothesis may not survive. But it seems likely that these subtle details in the harmonic structure carry useful information about the structure of the disk, and warrant further study.

## 6. SUPERHUMP PERIOD CHANGES, AND LATE SUPERHUMPS

We measured all light curves for times of maximum light in the superhump cycle. The identification of hump maximum was ambiguous in a few cases, and required pre-subtraction of the mean orbital signal during the week after the rapid decline (Figure 5). But with these omissions and qualifiers, we present the timings in Table 2.

Figure 6 is an O–C diagram of these timings, relative to the test ephemeris HJD 2451562.2807 + 0.07583 *E*. The initial portion of Figure 6, covering JD 62–68, suggests a parabolic term indicative of a small period decrease. The fitted parabola corresponds to the ephemeris

$$\text{Superhump maximum} = \text{HJD } 2{,}451{,}562.2880 + 0.07599\,E - 2.0\times10^{-6}\,E^2, \quad (1)$$
$$(20) \quad (9) \quad (0.9)$$

which signifies a (marginal) rate of period decrease $\dot{P} = -5(\pm2)\times10^{-5}$. This is the usual pattern seen in the common superhumps of dwarf novae. After JD 69.0 the points stagger rapidly upward in O–C, then resume a downward drift.

Fitting the entire O–C for best period, we find $P$=0.07596(5) d, with a fit that is really not credible (since the curve *never* conforms locally to that value!). But the episode of rapid movement in O–C occurred just when the star staged its rapid decline on JD 69–70, and this suggests an alternative description. Namely, the description implied by the fitted sections of O–C curve in Figure 6: separate regimes on either side of the rapid decline, with a phase shift of 0.58±0.07 cycles (allowing for uncertainties in the extrapolated slopes of the two curves).

On general principles of curve-fitting, it would be difficult to recommend this fitting scheme, since it violates Ockham's Razor (*hypotheses non multiplicanda sine necesitate*, Ockham c. 1320). But guidance may be sought in studies of other stars, and this description follows a pattern that has become familiar in the better-studied superhumping dwarf novae. It was first found by Vogt (1983) in VW Hyi, where it appeared practically identical to the syndrome described here: a very strong signal at $P_{sh}$ which followed the rapid decline, accompanied an orbital wave, and showed a phase shift of ~0.5 cycles from the common superhumps. Vogt called these "late superhumps". A very thorough study in VW Hyi was reported by van der Woerd et al. (1988). Such waves have also been prominently seen in OY Car (Schoembs 1986, Hessman et al. 1992) and EG Cnc (Patterson et al. 1998), and probably also in V1159 Ori (Patterson et al. 1995) and SU UMa (Udalski 1990).

In view of all the resemblances to the late-superhump syndrome, it seems likely that after the rapid decline on JD 69–70, IY UMa showed a combination of late superhumps and the normal orbital wave. We shall henceforth adopt this description. The fitted straight line in Figure 6 corresponds to

$$\text{Late superhump maximum} = \text{HJD } 2{,}451{,}571.731 + 0.07558\,E. \quad (2)$$
$$(3) \quad (6)$$

## 7. THE ECLIPSES

The most interesting aspect of IY UMa is certainly the deep eclipses, which offer a powerful probe of the spatial extent of the light source. For all early eclipses of adequate signal-to-noise, we measured the following quantities:

$t_1$ = first contact
$t_i$ = half-light on ingress
$t_{min}$ = minimum light
$t_e$ = half-light on egress
$t_4$ = last contact
depth = eclipse depth reckoned by interpolating between $t_1$ and $t_4$

and present them in Table 3.

From visual inspection of the light curves, it is obvious that the eclipse depth is strongly affected by the location of the superhump: eclipses are shallow when hump maximum coincides with eclipse. This is demonstrated in Figure 7, where the eclipse depth is plotted against beat phase of orbit and superhump. Zero beat phase is the phase at which hump maximum coincides with eclipse.

After the star faded and the eclipse changed to a more intricate shape, we measured somewhat different quantities, as illustrated in Figure 8:

$t_1$ = first contact
$t_{wdi}$ = white dwarf mid-ingress
$\Delta t_{wdi}$ = duration of white dwarf ingress
$\Delta I_{wdi}$ = white dwarf light eclipsed on ingress
$t_{min}$ = minimum light
$t_{wde}$ = white dwarf mid-egress
$\Delta t_{wde}$ = duration of white dwarf egress
$\Delta I_{wde}$ = white dwarf light uncovered on egress
$t_{hse}$ = hot-spot mid-egress
$\Delta t_{hse}$ = duration of hot-spot egress
$\Delta I_{hse}$ = hot-spot light uncovered on egress
$t_4$ = last contact
depth = eclipse depth reckoned by interpolating between $t_1$ and $t_4$

The measured quantities are presented in Table 4, along with their nightly averages. In preparing this table, we converted all light curves to intensity units, and transformed to "*BG*" intensities using the episodes of simultaneous *B*/*V*/*BG* coverage. *B*=20.0 corresponds to a *BG* intensity = 3.13. (Thus the white dwarf, when first detected on JD 70, has an intensity of 40 and hence *B*=17.24.)

Most of the measurements were straightforward, except for the durations of white-dwarf

ingress and egress. The integration time was typically half of these durations, making the time resolution quite coarse. We obtained 25±5 s from a weighted average over all data. However, the inevitable gentle roll-over of the light curve near first and fourth contacts (of the white dwarf) is not observable in data of this signal-to-noise. We studied how this effect would degrade the estimate in the case of a binary where the answer is well-known (V471 Tau, Warner et al. 1971). By adding flickering and photon-counting noise to V471 Tau, we estimated that the full duration in IY UMa should be increased to 29±5 s.

The times of white dwarf mid-ingress and mid-egress are stable, as is their difference (412±4 s). The average of these times defines mid-eclipse (superior conjunction of the white dwarf), which follows the ephemeris

$$\text{White dwarf mid-eclipse} = \text{HJD } 2{,}451{,}570.85376(2) + 0.07390906(7)E. \quad (3)$$

This is a very exact indicator of true dynamical conjunction, so we use it as the orbital phase convention in this paper.

We combined orbital and superhump ephemerides to generate "precession" ephemerides[3], using the coincidence of superhump maximum and mid-eclipse as the zero-marker of phase:

$$\text{Precession phase zero} = \begin{array}{l} 61.985 + 2.90\,E \text{ (common, JD 62–70)} \\ 72.184 + 3.34\,E \text{ (late, JD 72–79).} \end{array} \quad (4)$$

We then converted all the events in Tables 3 and 4 to orbital phase and precession phase (which we designate as Φ), and looked for correlations with Φ. The results for the common superhump are shown in Figure 9. All the eclipse timing markers show a similar dependence: eclipse minimum varies by 0.0088±0.0015 cycles, occurring latest at Φ=0.68±0.05; last contact ($\varphi_4$) varies by 0.039±0.006 cycles, occurring latest at Φ=0.52±0.06; half-ingress varies by 0.016±0.004 cycles, occurring latest at Φ=0.56±0.07; and, half-egress varies by 0.012±0.005 cycles, occurring latest at Φ=0.60±0.10. Thus each of these independent measures indicates a left-right asymmetry in disk light which varies with precession phase — as would be produced by a slowly precessing elliptical disk. We summarize these variations by saying that the eclipse markers occur latest at Φ=0.59±0.05.

The eclipses occur on a background that is sloped due to the superhump, so this was subtracted prior to all measurements. We remeasured without this subtraction, to check sensitivity to this technique. No substantial and systematic changes were found; the slopes due to eclipse are generally greater than that due to the superhump, so this is not a dominant effect.

Calculating eccentricity from the observed asymmetries depends on specific assumptions about the disk (e.g., brightness dependence on radius), so this is not easy. The exception is $\varphi_4$,

[3] Precession is used here merely to denote the beat cycle of the two observable clocks, not to assume or require any specific interpretation. However, the periodic variations found below are consistent with a precessing ellipse, so perhaps we can soon use the term without apology!

which is at least in principle a pure measure of the disk edge (although difficult to measure since first and last contacts are contaminated by flickering). From the observed variation in $\varphi_4$ we estimate $e$=0.29±0.06.

The other interesting aspect of these measurements is that they are not symmetric about $\varphi$=0. Minimum light is symmetric about $\varphi$=0.0042±0.0010. We can also consider the quantities $\varphi_4+\varphi_1$ and $\varphi_i+\varphi_e$; these are easily derived from Table 2 and are sensitive probes of the eclipse symmetry. We found that the former is symmetric about 0.017±0.003, and the latter is symmetric about 0.009±0.003. The positive mean in all these quantities implies that the disk's light is asymmetric in the sense that the leading lune, the side eclipsed after the white dwarf, is brighter.

There is no clear reason for the disk itself to produce this asymmetry. In the most popular understanding of dwarf-nova outbursts, light is produced by sudden accretion through the disk from an accretion ring that has been accumulating matter since the last outburst, with no need for enhanced mass transfer from the secondary (Osaki 1996). This light should be symmetric about the white dwarf (precession is irrelevant here since we are only concerned with the mean residual, averaged over the precession cycle). This expectation appears to conflict with the data. But a quite simple way to preferentially light up the leading lune is to hypothesize mass transfer at a high rate. The resultant hot spot in the leading lune is what drives the eclipses slightly late, relative to true dynamical conjunction, in essentially all high-$\dot{M}$ disk accretors (see Figure 9 of Nather & Robinson 1974). Of course, very high binary inclination exaggerates the effect considerably, since it dims the disk and enhances the hot spot. It would be very interesting to calculate the size of this effect as a function of accretion rate, mass-transfer rate, and inclination.

## 8. WHITE DWARF CHANGES

The bright central object first emerged in the light curve on JD 70, just after the rapid decline. Detailed measurement of this object continued for another 60 days, and the nightly averages (bottom of Table 4) show that its brightness and ingress/egress durations varied. The trends are shown in the lower frames of Figure 10. Here we use the nightly averages with both ingress and egress merged, but assign triple weight to the measurements during egress, since at that time the covered hot spot does not compete, giving a more accurate and repeatable measurement.

During the week following rapid decline, the egress duration fell rapidly from ~40 s to 25±5 s, and remained sensibly constant thereafter. (We omit the correction to 29±5 s suggested above, as this arguably systematic error should not affect the observed *changes*.) The spectroscopy reported below revealed broad H absorptions characteristic of a white dwarf photosphere, so this small bright object at disk center is evidently the white dwarf. With the white-dwarf magnitudes reported below ($B$=18.02, $I$=17.77 on JD 105), we estimate from empirical calibrations and model atmospheres a corresponding $B$–$V$=0.10±0.08 and hence $T_{\rm eff}$=14,500±1600 K (Koester et al. 1979).

Prior to JD 76, Figure 10 shows that the eclipsed object was definitely bigger, by up to

~50%. What is this object that mimics a white dwarf but is too large? Well, on JD 69, the day previous to the central object's sudden apparition, the light curve was utterly smooth and dominated by the disk. Since matter in the luminous inner part of disks clears out by spiraling *inward*, it seems plausible that this is merely the remnant of the optically thick disk, which disappeared between JD 74 and 76.

The variation of central-object brightness, in the middle frame of Figure 10, is more interesting. These points are much more accurate (with errors about the symbol size) than the egress durations, and suggest continued fading of the white dwarf even after the duration appears to level off to a constant. This implies *cooling* of the white dwarf. The white dwarf fades about 30% in blue light between JD 76 and 102, which implies about a 12% decline in temperature if $T$ is near 14000 K.

## 9. BINARY PARAMETERS FROM ECLIPSES

With a precise measurement for the duration of the white-dwarf eclipse, it is easy to derive a $q(i)$ constraint from Roche geometry and Kepler's Third Law (Chanan, Middleditch, & Nelson 1978). The timings of hot-spot ingress and egress depend sensitively on $q$, so we used the method of Wood et al. 1986 (see also Smak 1971, Smak 1979, Cook & Warner 1985) to measure $q$=0.13±0.02 and $R_{disk}/a$=0.28±0.02 from the observed binary phases (–0.0080, +0.0769). Finally we have a 29±5 s constraint for the white-dwarf eclipse, mostly arising from the size of the white dwarf; for the analysis of binary parameters, we used an analytic mass-radius relation for a zero-temperature white dwarf (Nauenberg 1972).

The shaded region in Figure 11 shows the resultant constraints on $M_2$ and $M_1$. The solution is $M_2$=0.12±0.03 $M_\odot$, $M_1$=0.85±0.12 $M_\odot$, and $i$=86.8±1.5°. Below we will find slightly tighter limits, indicated by the black figure, incorporating a (less certain) luminosity argument.

## 10. DISTANCE AND LUMINOSITY

The most useful distance constraint comes from the empirical correlation between $P_{orb}$ and $M_V$ at the peak of a normal eruption (Vogt 1981, Warner 1987). IY UMa has $V$=14.1±0.2 at the peak of this superoutburst, and normal eruptions among this class of stars peak at ~0.5 mag fainter; thus we estimate $V$(max)=14.6±0.4. At the likely inclination of $i$=86°, the disk light in eruption is diminished by ~2.5 mag relative to the "standard inclination" of $i$=56° (Mayo et al. 1980, Warner 1995). Allowing an additional uncertainty of 0.7 mag for the inclination correction, we adopt a corrected $V$(max)=12.1±0.8. The empirical correlation predicts ($M_V$)max=5.4±0.3 at $P_{orb}$=1.8 hr (Figure 3.10 of Warner 1995). Neglecting interstellar extincion, we then estimate a distance of 220±70 pc.

The white-dwarf magnitudes deduced from eclipse supply an independent constraint. On JD 105, long after the eruption ended, the white dwarf had $B$=18.02 and $I$=17.77 (both ±0.05), with this color suggesting $T_{eff}$=14,500±1600 K. For white dwarfs of this temperature and in the deduced mass range, we estimate a distance of 160±60 pc. Thus the distance estimates from "white-dwarf parallax" and "dwarf-nova parallax" converge on 190±60 pc.

The multicolor light curves constrain the secondary too. Useful constraints can be found from the deep eclipse, and from the guarantee (owing to the very high *i*) that the secondary's intrinsic light must show an "ellipsoidal" variation with ~0.30 mag full amplitude. Figure 12 shows the folded *B* and *I* orbital light curves on JD 105. Six eclipses in quiescence show that IY UMa reaches $I$=17.74±0.06 at mid-eclipse, setting a limit $I_{sec}$>17.6 (the narrow side of the secondary faces Earth at this phase, so a 0.15 mag adjustment is needed to obtain an orbit average). Away from eclipse, the star averages $I$=16.34 and displays an orbital waveform similar to the waveform in *B* light, where the secondary is of no consequence at all. So the secondary is definitely a very minor contributor in *I* light at quiescence. After subtracting the white dwarf (measured at $I$=17.77 from the eclipse, and assumed to be constant over the binary orbit) and excluding the large orbital hump, we obtain $I$=16.97 for the remaining light, and estimate that at most 40% of it can have the required double-humped dependence on orbital phase.[4] This implies $I_{sec}$>18.0. Finally, we note that the color of the light at mid-eclipse is quite red ($B$=19.9, $I$=17.7), probably too red to be dominated by accretion light. Thus it is plausible that the *I* brightness of the secondary lurks not far from the limit quoted above. We consider $I_{sec}$=18.7±0.5 to be a reasonable guess.

At 190±60 pc, this implies that the secondary has $M_I$ =11.4–13.3. In current models of single low-mass stars of solar composition (Burrows et al. 1989, Chabrier & Baraffe 1997), this corresponds to $M_2$=0.10–0.13 $M_\odot$. This gives the somewhat better constrained black polygon in Figure 11. The gray region is still available, though, if the secondary's light is *not* a major component of the *I* light at mid-eclipse.

## 11. SPECTROSCOPY AT QUIESCENCE

We obtained spectra of IY UMa on 2000 April 7 and 10 UT, using the 2.4 m Hiltner telescope at MDM Observatory. The modular spectrograph and a $2048^2$ thinned SITe CCD detector were used, giving ~3.5 Å resolution from 4200 to 7500 Å, with severe vignetting near the ends of the range and degradation of focus at the blue end. Variable seeing (creating uncalibrated light losses at the 1 arc-second slit) and thin clouds persisted through most of the observations, which covered three binary cycles and five eclipses. Most exposures were 240 s, with some shorter ones near eclipse. We took comparison lamp exposures at least once per hour, observed flux standard stars, and reduced the data to flux versus wavelength.

For each eclipse, we timed a 200–240 s exposure to coincide with mid-eclipse, accumulating 1160 s of such exposure. During eclipse the telescope was guided by hand, using a nearby faint field star visible on the slit jaws; some centering error is likely. The signal-to-noise was low, with the continuum level equivalent to $V$=19.7. Comparison with M4/M5 dwarf spectra establishes that less than half of the *V*-band flux at mid-eclipse arises from the secondary. (The

[4] This limit may seem crude, since the double-humped signature is altogether invisible. But on that night the *B* light curve, thought to express the radiation pattern of the hot spot, showed some wiggles roughly anti-phased with the ellipsoidal wiggles expected from the secondary. This coarsens the upper limit.

resultant $V_{sec}$>20.4 corresponds to $I_{sec}$>17, so this is consistent with the above photometry.)

Figure 13 shows the mean spectrum. The Balmer emission is strongly double-peaked, with the components separated by 1400±200 km/s. The many He I lines (λλ4921, 5015, 5876, 6678, 7065) show absorption going beneath the continuum. The Hβ emission resides in a broad absorption trough with an equivalent width of ~30 Å. This is approximately the trough expected with the white dwarf parameters deduced from photometry [~60 Å from a log $g$=8, 14000 K white dwarf (Koester et al. 1979), diluted by the ~50% of 5000 Å continuum light not arising from the white dwarf]. A blue spectrum from the Nordic Optical Telescope showed higher Balmer absorptions also consistent with this temperature (Abbott 2000, priv. comm.).

Figure 14 shows single-trailed spectrograms of the regions near Hα and He I λ5876, constructed with the phase-smoothing procedures described by Taylor et al. (1999). Both lines show prominent *S*-waves, with a semi-amplitude of 750±60 km/s and maximum recessional velocity at φ=0.10±0.02. (Unfortunately, this wave confounded our attempt to measure a traditional *K*-velocity.) Hα also shows a strong "rotational disturbance" across eclipse, indicating that the double-peaked emission arises from a disk in prograde rotation. There is also weak absorption near the rest wavelengths of the NaD lines (5889 and 5895 Å). Finally, there is unidentified weak emission near λ5861, and probable absorption near λ5912, each with a dependence on orbital phase. The properties of the *S*-wave, including its phasing and near-disappearance in 0.3<φ<0.6, are consistent with an origin in the hot spot, as commonly seen in quiescent dwarf novae (Smak 1985).

To wring some more information from the *S*-wave, we modelled the stream trajectory by integrating a particle trajectory in the Roche potential.[5] Using the central values from the photometric analysis ($M_1$=0.85 $M_\odot$, $M_2$=0.11 $M_\odot$, $i$=86.8°), we found the results seen in Figure 15. Dotted arrows show the gas-stream free-fall velocity viewed by a non-corotating observer, and solid arrows show the Keplerian disk velocity under the location of the gas stream (of course, it is an open question whether there is any disk at that location; that's the point of the calculation!). Comparing these to the observed amplitude and phase of the *S*-wave, indicated at the lower left of Figure 15, shows that for the observed amplitude, the phase corresponds well to the Keplerian velocity, with some mixture of free-fall velocity. The computed speed best matches 750 km/s for $R_{disk}/a$=0.28±0.03. This location is shown by the "+" symbol in Figure 15; comparison with the values estimated from eclipse in the common-superhump and late-superhump eras (0.44 and 0.35) is consistent with the general idea that the disk shrinks during the decay from eruption.

## 12. SUMMARY

1. We report detailed light curves of IY UMa obtained during and after the January 2000 superoutburst. The star is a deeply eclipsing dwarf nova of the SU UMa type, with an out-of-eclipse magnitude in the range $V$=14.0–17.3. The orbital period is 0.0739091(1) d, with times of dynamical conjunction very precisely specified by the white dwarf eclipses.

[5] Analysis based on Doppler tomograms gave a similar result.

2. There are powerful superhumps at a period of 0.07583 d, 2.6% longer than $P_{orb}$. The period decreased slightly ($\dot{P} = -5\times10^{-5}$) during the superoutburst, as is typical for the common superhumps of dwarf novae. After the rapid decline, the humps grew in amplitude and changed phase by ~0.5 cycles, as is typical for late superhumps. In addition to the main signal at $\omega_o-\Omega$, the common and late superhumps showed an intricate fine structure at higher frequency, including signals at $3\omega_o-\Omega$, $4\omega_o-\Omega$, and $5\omega_o-\Omega$ (where $\omega_o$ and $\Omega$ are respectively the orbital and "precession" frequencies).

3. During outburst, the wide and smooth eclipses signify a large accretion disk, with $<R_{disk}/a>=0.44\pm0.03$. The eclipses show large changes in disk shape which appear to be cyclic with the putative precession period of 2.9 d. From timings of last contact, we estimate an eccentricity $e=0.29\pm0.06$. Other timing signatures are systematically late, probably driven by the mass-transfer hot spot.

4. After the rapid decline, the eclipses changed their structure and revealed two small bright sources in the binary: the white dwarf and the hot spot. They also became much narrower, suggesting that $R_{disk}$ declined by ~20–30%. A separate study of eclipse timings in this "late-superhump" era showed evidence for accretion-disk precession with a mean disk radius given by $R_{disk}/a=0.35\pm0.04$ (Rolfe, Haswell, & Patterson 2000).

5. During quiescence, the knife-edge of the secondary traverses the white dwarf in 29±5 s. A photometric eclipse analysis gave $M_2=0.12\pm0.02\ M_\odot$, $M_1=0.86\pm0.11\ M_\odot$, $i=86.8\pm1.5°$. We estimate $T_{eff}=14{,}500\pm1600$ K for the white dwarf, cooling slightly after the outburst.

6. Arguments from the observed brightness of the white dwarf and the accretion disk in eruption converge on a distance estimate of 190±60 pc.

7. Spectroscopy at quiescence showed a typical spectrum of a low-$\dot{M}$ dwarf nova seen at high inclination, with strongly double-peaked lines and a rotational distortion in eclipse. A strong *S*-wave reached maximum velocity of recession at $\varphi=0.10\pm0.02$. Broad absorptions from the white dwarf were consistent with the temperature deduced from photometry. The phase and amplitude of the *S*-wave indicated an origin in Keplerian motion at the hot spot with $R_{disk}/a=0.28\pm0.02$.

8. As a dwarf nova of long recurrence period and yet only a modest amplitude of ~3.3 mag, IY UMa flagrantly violates the famous period-amplitude relation (Kukarkin & Parenago 1934). The reason almost certainly lies in the binary inclination. At $i=86°$ the disk in eruption is extremely foreshortened and thus dimmed (by 2.5±0.7 mag as estimated above). Only the flat, optically thick disk requires this correction; the various light sources at quiescence (white dwarf, hot spot, secondary, optically thin disk) do not. Thus the corrected amplitude is ~6 mag, a typical value for dwarf novae of very long recurrence period.

9. It is hard to imagine a better accretion laboratory than IY UMa: a nearby star with high and low states, clear lines of sight to the central object, vigorous superhumps, a very high binary

inclination (and hence the great diagnostic power of eclipses), and distinct eclipse signatures of the different components in the binary. We eagerly await the harvest this star seems certain to bestow upon us!

Improvements in technology and communication have made feasible what would have been extraordinary or impossible just a few years ago. Backyard observers are now finding — visually or with CCD cameras — faint and rare eruptions in the early stages, and we depended completely on Schmeer's wonderful discovery. Instant worldwide communication was also necessary, and we were greatly aided by the vigilance, speed, and reliability of the VSNET e-mail service from Kyoto University. So were many other observers; there may be debate about what triggers dwarf-nova outbursts, but there can be no debate about what triggers avalanches of variable-star observations. In this little universe, who rules the internet rules the backyard. We are also grateful to the Research Corporation (grant GG385) and the National Science Foundation (grant AST96–18545) for their support of CBA science.

## REFERENCES

Burrows, A., Hubbard, W.B., Lunine, J.I. 1989, ApJ, 345, 939.
Chabrier, G. & Baraffe, Y. 1997, A&A, 327, 1039.
Chanan, G.A., Nelson, J.E., & Middleditch, J. 1978, ApJ,
Cook, M.C. & Warner, B. 1984, MNRAS, 207, 705.
Henden, A.A. 2000, vsnet-alert, 4060 (http://www.kusastro.kyoto-u.ac.jp/vsnet/Mail/vsnet-alert/msg04060.html).
Hessman, F.V., Mantel, K.H., Barwig, H., & Schoembs, R. 1992, A&A, 263, 147.
Horne, K., Wood, J.H., & Stiening, R.F. 1991, ApJ, 378, 271.
Koester, D., Weidemann, V., & Schulz, H. 1979, A&A, 76, 262.
Kukarkin, B.V., & Parenago, P.P. 1934, *IBVS*, 4, 44.
Lubow, S.H. 1991, ApJ, 381, 268.
Mayo, S.K., Wickramasinghe, D.T., & Whelan, J.A.J. 1980, MNRAS, 193, 793.
Nather, R.E. & Robinson, E.L. 1974, ApJ, 190, 637.
Nauenberg, N. 1972, ApJ, 175, 417.
Ockham, W. of, c. 1320, *Tractatus de sacramento altaris* (Parisiis), tr. T.B. Birch 1930 (Burlington, Iowa: Lutheran Literary Board).
O'Donoghue, D. 1986, MNRAS, 220, 23.
O'Donoghue, D. 1990, MNRAS, 246, 29.
Osaki, Y. 1989, PASJ, 41, 1005.
Osaki, Y. 1996, PASP, 108, 39.
Patterson, J. 1981, ApJS, 45, 517.
Patterson, J. 1998, PASP, 110, 1132.
Patterson, J., Jablonski, F., Koen, C., O'Donoghue, D., & Skillman, D.R. 1995, PASP, 107, 1183.
Patterson, J. et al. 1998, PASP, 110, 1290.
Ritter, H. & Schroeder, R. 1979, A&A, 76, 168.
Rolfe, D.J., Haswell, C.A., & Patterson, J. 2000, MNRAS, submitted.
Robinson, E.L. et al. 1995, ApJ, 443, 295.
Russell, H.N. & Shapley, H. 1912, ApJ, 36, 239.
Schmeer, P. 2000, vsnet-alert, 4027 (http://www.kusastro.kyoto-u.ac.jp/vsnet/Mail/vsnet-alert/msg04027.html).
Schoembs, R. 1986, A&A, 158, 233.
Simpson, J.C. & Wood, M.A. 1998, ApJ, 506, 360.
Skillman, D.R. et al. 1999, PASP, 111, 1281.
Skillman, D.R. & Patterson, J. 1993, ApJ, 417, 298.
Smak, J.I. 1971, Acta Astr., 21, 15.
Smak, J.I. 1985, Acta Astr., 35, 351.
Udalski, A. 1990, AJ, 100, 226.
Uemura, M. et al. 2000, PASJ, in press.
van der Woerd, H., van der Klis, M., van Paradijs, J., Beuermann, K., & Motch, C. 1988, ApJ, 330, 911.
Vogt, N. 1983, A&A, 118, 95.
Warner, B. 1974, MNRAS, 168, 235.
Warner, B. 1985, in Interacting Binaries, ed. P.P. Eggleton and J.E. Pringle (Dordrecht: Reidel),

p. 367.
Warner, B. 1987, MNRAS, 227, 23.
Warner, B. 1995, Cataclysmic Variable Stars (Cambridge: Cambridge Univ. Press).
Warner, B., Robinson, E.L., & Nather, R.E. 1971, MNRAS, 154, 455.
Whitehurst, R. 1988, MNRAS, 232, 35.
Wood, J.H., Horne, K., Berriman, G., Wade, R.A., O'Donoghue, D., & Warner, B. 1986, MNRAS, 219, 619.
Wood, J.H., Horne, K., Berriman, G., & Wade, R.A. 1989, ApJ, 341, 974.

TABLE 1
LOG OF PHOTOMETRIC OBSERVATIONS

| HJD Start (2,451,500+) | Duration (hr) | Tel.[a] | Filter | Points | <*V*> | HJD Start (2,451,500+) | Duration (hr) | Tel.[a] | Filter | Points | <*V*> |
|---|---|---|---|---|---|---|---|---|---|---|---|
| 62.2170 | 11.33 | 1 | *C* | 327 | 14.31 | 71.78387 | 2.08 | 6 | *BG* | 350 | |
| 62.8438 | 5.59 | 2 | *V* | 403 | 14.20 | 71.88629 | 2.30 | 6 | *C* | 587 | |
| 63.7133 | 8.89 | 2 | *V* | 823 | 14.10 | 71.98742 | 2.03 | 6 | *U* | 341 | |
| 63.7151 | 1.83 | 3 | *C* | 113 | 14.14 | 72.66888 | 7.20 | 6 | *B* | 1030 | |
| 64.3198 | 7.02 | 1 | *C* | 195 | 14.35 | 72.89381 | 2.45 | 2 | *V* | 180 | 16.66 |
| 64.92762 | 1.62 | 2 | *V* | 167 | 14.47 | 73.9353 | 3.09 | 2 | *V* | 254 | 16.96 |
| 65.7001 | 3.46 | 4 | *C* | 383 | | 73.65927 | 9.60 | 6 | *BG* | 1618 | 16.80 |
| 66.68613 | 9.51 | 2 | *V* | 999 | 14.42 | 74.0239 | 0.76 | 2 | *B* | 44 | |
| 67.2157 | 12.37 | 1 | *C* | 358 | 14.71 | 74.68093 | 7.99 | 6 | *BG* | 800 | 16.95 |
| 67.7500 | 2.77 | 2 | *V* | 289 | 14.79 | 74.97394 | 2.11 | 2 | *V* | 126 | 16.62 |
| 68.2409 | 5.37 | 5 | *C* | 283 | 14.87 | 76.68799 | 5.68 | 2 | *BG* | 1037 | 16.84 |
| 68.69055 | 9.14 | 2 | *V* | 1100 | 14.88 | 76.6887 | 8.06 | 3 | *C* | 492 | |
| 69.2470 | 5.40 | 5 | *C* | 163 | 14.96 | 77.7081 | 8.11 | 3 | *C* | 352 | 17.00 |
| 69.68465 | 7.23 | 2 | *V* | 685 | 15.16 | 78.63061 | 7.20 | 2 | *BG* | 1255 | 16.94 |
| 70.6214 | 3.48 | 5 | *C* | 53 | 16.00→16.22 | 84.81402 | 4.81 | 6 | *BG* | 801 | 17.10 |
| 70.67161 | 9.47 | 2 | *V* | 1000 | 16.10→16.56 | 100.98720 | 1.50 | 2 | *BG* | 511 | 16.91 |
| 71.4559 | 7.29 | 5 | *C* | 96 | 16.70 | 101.98211 | 1.80 | 2 | *BG* | 608 | 17.01 |
| 71.6469 | 7.83 | 4 | *C* | 379 | | 104.59516 | 1.97 | 2 | *I* | 613 | |
| 71.69737 | 8.96 | 2 | *V* | 1086 | 16.55 | 104.82565 | 4.37 | 2 | *BG* | 1141 | 16.96 |
| 71.68034 | 2.47 | 6 | *B* | 416 | | 105.64006 | 5.51 | 2 | *B, I* | 587 | |

[a] Telescope: 1 = CBA–Denmark 0.25 m; 2 = MDM 1.3 m; 3 = Braeside 0.4 m; 4 = CBA–East 0.66 m; 5 = CBA–Belgium 0.35 m; 6 = MDM 2.4 m.

TABLE 2
TIMES OF SUPERHUMP AND ECLIPSE

| Superhump Maxima (HJD 2,451,500+) | | | | | |
|---|---|---|---|---|---|
| 62.2850 | 64.3397 | 67.2949 | 68.654 | 70.953 | 76.870 |
| 62.3618 | 64.4102 | 67.3699 | 68.7346 | 71.028 | 76.947 |
| 62.4400 | (64.4885) | 67.4428 | 68.8850 | 71.733 | 77.025 |
| 62.5149 | (64.5710) | 67.5206 | 69.277 | 71.806 | 77.780 |
| 62.5927 | (64.9455) | (67.595) | 69.346 | 71.959 | 77.853 |
| 62.6702 | (65.7040) | (67.672) | 69.421 | 72.033 | 77.927 |
| 62.9730 | 65.7786 | (67.750) | 69.7368 | 73.690 | 78.004 |
| 63.0479 | 66.6961 | 67.830 | 69.8128 | 73.768 | 78.685 |
| 63.7343 | 66.8435 | 68.277 | 70.653 | 73.843 | 78.758 |
| 63.8105 | 66.9188 | 68.353 | * | 73.916 | 78.831 |
| 63.8846 | 66.9940 | 68.428 | 70.729 | 74.840 | 78.907 |
| 63.9613 | 67.0701 | 68.505 | 70.802 | 74.989 | |
| 64.0357 | 67.2171 | 68.583 | 70.876 | 76.804 | |

* Timings after the asterisk were calculated after pre-subtraction of the mean orbital light curve.

| White-Dwarf Mid-Eclipse (HJD 2,451,500+) | | | | | |
|---|---|---|---|---|---|
| 70.70584 | 71.81457 | 72.84938 | 76.76650 | 78.90988 | 104.92581 |
| 70.77987 | 71.88848 | 72.92322 | 76.84043 | 84.82258 | 105.66480 |
| 70.85368 | 71.96235 | 73.73625 | 76.91436 | 84.89650 | 105.73883 |
| 70.92757 | 72.03627 | 73.88404 | 78.68813 | 84.97040 | 115.71632 |
| 71.00154 | 72.70149 | 74.03164 | 78.76207 | 101.00863 | 123.92052 |
| 71.74065 | 72.77547 | 76.69262 | 78.83598 | 102.04340 | |

TABLE 3
ECLIPSE MEASUREMENTS IN SUPEROUTBURST

| $t_1$ | $t_i$ | $t_{min}$ | $t_e$ | $t_4$ | depth |
|---|---|---|---|---|---|
| (HJD 2,451,500+) | | | | | (mag) |
| 62 | | .4239 | | | 0.95 |
| 62.8650 | .8688 | .8718 | .8746 | .8789 | 1.64 |
| 63.0138 | .0169 | .0195 | .0225 | .0276 | 1.50 |
| 63.7522 | .7561 | .7589 | .7625 | .7660 | 1.21 |
| 63.8998 | .9037 | .9067 | .9100 | .9139 | 1.33 |
| 63.9729 | .9774 | .9808 | .9844 | .9882 | 1.31 |
| 64.0475 | .0513 | .0547 | .0579 | .0618 | 1.37 |
| 64.9351 | .9375 | .9411 | .9441 | .9465 | 0.99 |
| 65 | .7509 | .7540 | .7576 | .7638 | 1.94 |
| 66.7086 | .7124 | .7154 | .7189 | .7238 | 1.63 |
| 66.7828 | .7863 | .7892 | .7928 | .7974 | 1.64 |
| 66.8569 | .8606 | .8629 | .8663 | .8711 | 1.62 |
| 66.9304 | .9347 | .9370 | .9400 | .9445 | 1.52 |
| 67.0046 | .0083 | .0111 | .0140 | .0180 | 1.36 |
| 67 | | | | .7559 | 1.05 |
| 67.8158 | .8202 | .8235 | .8260 | .8289 | 1.00 |
| 68.3345 | .3375 | .3405 | .3436 | .3484 | 1.44 |
| 68.7767 | .7816 | .7844 | .7871 | .7920 | 1.92 |
| 69.0016 | .0037 | .0063 | .0090 | .0136 | 2.01 |
| 69.7393 | .7428 | .7458 | .7482 | .7533 | 2.05 |
| 69.8132 | .8167 | .8197 | .8221 | .8268 | 2.20 |

NOTES: $t_i$, $t_{min}$, and $t_e$ have an estimated error of 0.0002. $t_1$ and $t_4$ have an estimated error of 0.0003. Empty columns indicate that uncertainties exceeded this.

TABLE 4
ECLIPSE MEASUREMENTS AFTER SUPEROUTBURST

| $T_1$ (HJD[a]) | $t_{wdi}$ (HJD[a]) | $\Delta t_{wdi}$ (s) | $\Delta I_{wdi}$ | $t_{min}$ (HJD[a]) | $t_{wde}$ (HJD[a]) | $\Delta t_{wde}$ (s) | $\Delta I_{wde}$ | $t_{hse}$ (HJD[a]) | $\Delta t_{hse}$ (s) | $\Delta I_{hse}$ | $t_4$ (HJD[a]) | depth (mag) |
|---|---|---|---|---|---|---|---|---|---|---|---|---|
| Individual Measurements | | | | | | | | | | | | |
| 70.7028 | .70348 | 46 | 45 | .7068 | .70820 | 45 | 50 | .7110 | | 13 | .7118 | 2.08 |
| 70.7761 | .77748 | 55 | 37 | .7805 | .78226 | 36 | 45 | .7848 | | 10 | .7864 | 2.08 |
| 70.8502 | .85136 | 35 | 35 | .8545 | .85600 | 46 | 41 | — | | 12 | .8595 | 2.18 |
| 70.9247 | .92520 | 38 | 37 | .9284 | .92995 | 34 | 38 | — | | 9 | — | 2.10 |
| 70.9975 | .99919 | — | 36 | .0026 | .00389 | 35 | 32 | — | | 8 | .0075 | 2.23 |
| 71.7376 | .73830 | 53 | 38 | .7420 | .74300 | 53 | 31 | — | | 11 | .7487 | 2.07 |
| 71.7379 | | | | .7419 | .74304 | 37 | 28 | .7478 | 50 | 7 | .7494 | 2.59 |
| 71.8113 | | | | .8155 | .81698 | 41 | 28 | .8210 | 100 | 11 | .8217 | 2.52 |
| 71.8113 | .81225 | 54 | 33 | .8156 | .81688 | 46 | 36 | — | | 12 | .8218 | 2.21 |
| — | .88610 | 50 | 36 | .8893 | .89087 | 40 | 28 | — | | 14 | .8959 | 2.28 |
| 71.9580 | .95995 | 42 | 32 | .9633 | .96475 | 36 | 29 | .9690 | 110 | 12 | .9699 | 2.31 |
| 72.0330 | .03385 | 45 | 34 | .0371 | .03870 | 40 | 29 | .0432 | 60 | 13 | .0439 | 2.28 |
| 72.6975 | .69910 | 36 | 31 | .7027 | .70388 | 26 | 33 | .7074 | 38 | 23 | .7086 | |
| 72.7722 | .77313 | 33 | 25 | .7763 | .77782 | 35 | 31 | .7812 | 54 | 23 | .7821 | |
| 72.8462 | .84701 | 35 | 33 | .8502 | .85175 | 37 | 35 | .8551 | 40 | 14 | .8556 | |
| 72.9202 | .92083 | 35 | 31 | .9244 | .92561 | 36 | 30 | .9290 | 37 | 19 | .9303 | |
| 73.7333 | .73389 | 41 | 24 | .7371 | .73861 | 28 | 25 | .7418 | 40 | 7 | .7424 | 2.73 |
| 73.8800 | .88164 | 35 | 21 | .8852 | .88644 | 32 | 23 | .8897 | 50 | 5 | .8902 | 2.55 |
| 73.9543 | .95561 | 35 | 23 | | | | | | | | | |
| 74.0280 | .02936 | 30 | 24 | .0320 | .03392 | 40 | 24 | .0380 | 50 | 6 | .0382 | 2.00 |
| 74 | | | | .6978 | .69949 | 31 | 25 | .7040 | 52 | 5 | .7045 | 2.54 |
| 74.7678 | .76865 | 40 | 28 | | | | | | | | | |
| 74.9892 | | | | .9940 | .99506 | 30 | 26 | | | | | |
| 76.6895 | .69024 | 30 | 22 | .6937 | .69500 | 25 | 20 | .6979 | 43 | 7 | .6984 | |
| 76.7633 | .76414 | 21 | 24 | .7674 | .76887 | 22 | 21 | .7718 | 57 | 6 | .7726 | |
| 76.8374 | .83806 | 28 | 24 | .8413 | .84280 | 25 | 23 | .8459 | 38 | 6 | .8463 | |
| 76.9117 | .91198 | 19 | 24 | .9152 | .91674 | 19 | 23 | .9198 | 45 | 7 | .9201 | |
| 78.6848 | .68574 | 35 | 21 | .6894 | .69053 | 21 | 22 | .6945 | 58 | 15 | .6952 | |
| 78.7584 | .75970 | 27 | 25 | .7633 | .76445 | 24 | 22 | .7683 | 38 | 14 | .7695 | |
| 78.8315 | .83360 | 26 | 25 | .8374 | .83836 | 24 | 22 | .8421 | 42 | 16 | .8432 | |
| 78.9069 | .90749 | 24 | 23 | .9111 | .91227 | 20 | 21 | .9161 | 50 | 14 | .9172 | |
| 84.8195 | .82018 | 30 | 23 | .8237 | .82498 | 24 | 21 | .8287 | 36 | 5 | .8292 | |
| 84.8937 | .89412 | 34 | 21 | .8976 | .89887 | 26 | 21 | .9028 | 40 | 6 | .9032 | |
| 84.9672 | .96803 | 27 | 22 | .9716 | .97276 | 26 | 21 | .9766 | 42 | 4 | .9780 | |
| 101.0052 | .00626 | 18 | 19 | .0099 | .01101 | 19 | 18 | .0145 | 40 | 11 | .0150 | |
| 102.0407 | .04102 | | 17 | .0445 | .04577 | 27 | 18 | .0491 | 40 | 10 | .0492 | |
| 104.9232 | .92345 | 23 | 21 | .9268 | .92817 | 23 | 20 | .9316 | 30 | 8 | .9320 | |
| 105.6619 | .66260 | | | .6658 | .66700 | | | | | | | |
| Nightly Averages | | | | | | | | | | | | |
| 70.8503 | .85134 | 43 | 38 | .8546 | .85606 | 35 | 40 | .8588 | | 10.2 | .8598 | |
| 71.8849 | .88609 | 49 | 34 | .8895 | .89084 | 41 | 30 | .8952 | 78 | 12.4 | .8960 | |
| 72.7721 | .77306 | 35 | 30 | .7764 | .77781 | 34 | 32 | .7812 | 42 | 20 | .7822 | |
| 73.9543 | .95556 | 36 | 24 | .9587 | .96023 | 33 | 24 | .9637 | 50 | 6 | .9642 | |
| 74.7676 | .76865 | (40) | (28) | .7719 | .77337 | 30 | 25 | .7040 | (52) | 5 | .7045 | |
| 76.7635 | .76415 | 25 | 24 | .7674 | .76890 | 23 | 22 | .7719 | 46 | 6.5 | .7724 | |
| 78.7584 | .75968 | 28 | 23 | .7634 | .76445 | 22 | 22 | .7683 | 47 | 15 | .7693 | |
| 84.8935 | .89411 | 30 | 22 | .8976 | .89887 | 25 | 21 | .9027 | 39 | 5 | .9035 | |

[a]HJD = HJD 2,451,500+

## FIGURE CAPTIONS

FIGURE 1. — Light curve of IY UMa during the January 2000 superoutburst. Most points are orbital averages, accurate to <0.1 mag. The first four points (Schmeer 2000) are single measurements, with greater uncertainty. Still, the data establish that the eruption began on JD 2451556±2, and evolved on timescales very characteristic of SU UMa-type dwarf novae.

FIGURE 2. — Three 48-hour segments of light curve during superoutburst. Deep eclipses at $P_{orb}$ occur throughout. A prominent wave, the superhump, drifts slowly through the orbital light curve. The superhump amplitude and eclipse depth are periodically reduced when the superhump coincides with eclipse. Recurrent wiggles at higher frequency are also evident, especially in the last panel.

FIGURE 3. — Power spectrum of the JD 62–69 light curve, after removing eclipses. The four significant signals are marked with their frequencies in c/d, with an uncertainty of ±0.01 c/d. Three are simply components of the superhump at $\omega_s$=13.18 c/d, which is off scale with 700 units of power. Inset is the mean light curve, folded at this frequency. The 40.23 c/d peak is consistent with identification as $3\omega_o-\Omega$. We studied this region carefully to see if the peak could somehow be the result of a simple $3\omega_s$ signal viewed through the spectral window; the peak survived all these various exercises in skepticism.

FIGURE 4. — Nightly light curves of IY UMa after the rapid decline. A large wave of highly variable amplitude still exists. The eclipses are narrower, deeper, and sharper, with the sharpest features resolving the size and location of the white dwarf and hot spot.

FIGURE 5. — *Upper frame*, 9-night light curve after the rapid fall, with eclipses removed. The recurrent episodes of low wave amplitude suggest beating of closely spaced frequencies. *Middle frames*, power spectrum of this light curve (with eclipses removed), showing strong signals at 13.53 and 13.22 c/d — essentially the orbital and superhump frequencies — and three other frequencies coinciding with $3\omega_o$, $4\omega_o-\Omega$, $5\omega_o-\Omega$. *Lower frames*, mean post-eruption light curve, summed at the orbital and superhump periods.

FIGURE 6. — O–C diagram of the timings of superhump maxima, relative to the test ephemeris HJD 2451562.2807 + 0.07583 *E*. The first group are timings of the common superhump, fit by the parabola illustrated here and described by Eq. (1). After *E*=90, the timings climb by 0.58±0.07 cycles and appear to resume a downward drift — the familiar pattern of late superhumps. The transition between these eras occurred on JD 69–70 (see inset time scale), coinciding with the star's rapid decline.

FIGURE 7. — The correlation of eclipse depth with beat phase (between orbit and superhump cycles). Zero phase is the time when superhump maximum lines up with eclipse.

FIGURE 8. — Detail of one eclipse on JD 104, illustrating the timing signatures measured for each eclipse and entered in Table 4. The sharp eclipses are measured by mid-ingress and -egress (as well as duration and the step in intensity). Hot-spot ingress is usually difficult to measure,

although it becomes clear in a few cases (such as this light curve).

FIGURE 9. — Orbital phases of the eclipse timing signatures, as a function of precession phase during the common-superhump era. $\varphi_i$ and $\varphi_e$ are the orbital phases of half-light on ingress and egress; $\varphi_{min}$ is minimum light; and $\varphi_4$ is "last contact". All events show a smooth variation, occurring maximally late at $\Phi$=0.59±0.05. Ingress, egress, and eclipse minimum are symmetric about $\varphi$=0.005±0.001, indicating that the timings are also systematically late on average.

FIGURE 10. — *Lower frame*, variations in the white dwarf egress duration. Within measurement error, the egress lasts 25±5 s after JD 75. Earlier, the bright object at disk center is significantly larger. *Middle frame*, variations in white-dwarf brightness, reckoned in instrumental "*BG*" intensity units. Errors are equal to the symbol size. The brightness gradually drops, suggesting a cooling of the white dwarf by 15±4% over the 30 days of measurement (since the white dwarf emerged cleanly at JD 76). *Upper frame*, the eruption light curve for comparison. The bright object at disk center emerged abruptly at JD 70, just as the rapid decline phase ended; but it probably included a significant inner-disk contribution during JD 70–74.

FIGURE 11. — Binary constraints in the $M_2$–$M_1$ plane. The eclipse width of 412±4 s determines a $q(i)$ relation, and bounds on $q$ can be set from the hot-spot eclipse timings ($q$=0.13±0.02). These $q$ bounds set the top and bottom edges of the allowed space, which is shaded. The sides are set by bounds on the white dwarf's egress duration (29±5 s). A tighter constraint (black region) comes from a luminosity argument based on the probable detection of the secondary, but this is less secure.

FIGURE 12. — Simultaneous *B* and *I* orbital light curves on JD 105. 40 counts corresponds to *B*=17.97 and *I*=15.83. The similarity of light curves shows that the secondary is a very minor contributor to the out-of-eclipse *I* light. But the mid-eclipse light is quite red (*B*–*I*=2.2), suggesting that the secondary may contribute significantly at this phase.

FIGURE 13. — Mean spectrum in quiescence, showing strong doubled emission lines of H and He I, with a very broad absorption at Hβ.

FIGURE 14. — Single-trailed spectrograms in the vicinity of Hα and He I λ5876. A fitted continuum has been subtracted from the flux-calibrated spectrum. The gray scale is negative (dark = emission).

FIGURE 15. — A particle-trajectory model for the gas stream, computed for our nominal system parameters. Axes are referred to the system barycenter, and the plane of the figure is the orbit plane. Portions of the Roche critical lobes are shown. The 5-pointed star shows the white dwarf, and dots along the gas stream are separated by 10 s. The solid arrows represent the velocity of Keplerian rotation at each point indicated, as viewed by a non-corotating observer. The dotted arrows indicate the stream velocities in the same system (hence they are not tangent to the stream, but nearly tangent at high velocity). The observed phase and amplitude are indicated for reference at lower left. The cross indicates the location of the hot spot that best fits the phase and velocity, and occurs at $R_{disk}/a$ =0.28±0.02.

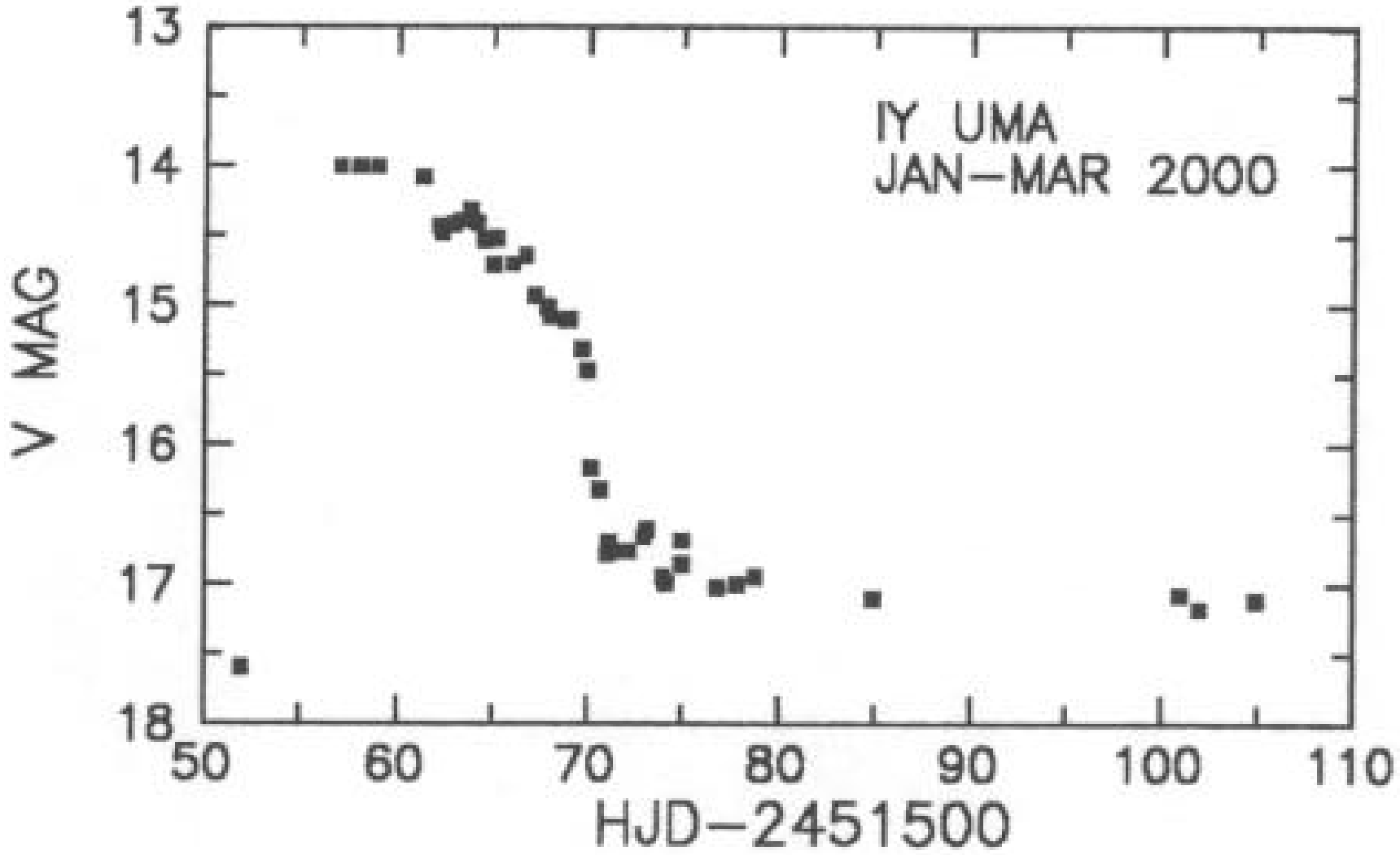
IY UMA
JAN–MAR 2000
V MAG
13
14
15
16
17
18
50
60
70
80
90
100
110
HJD–2451500

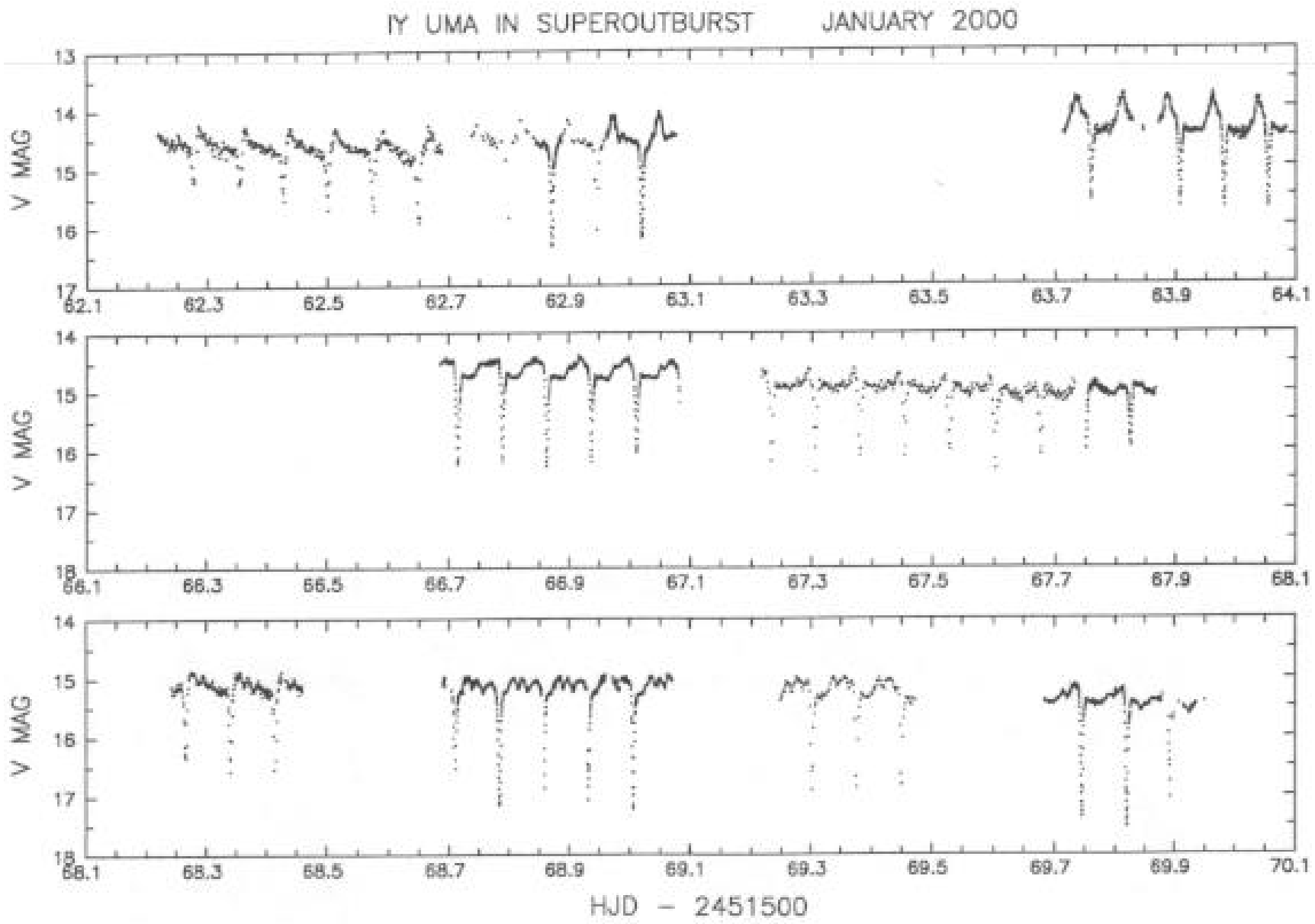
IY UMA IN SUPEROUTBURST JANUARY 2000
V MAG
13
14
15
16
17
62.1
62.3
62.5
62.7
62.9
63.1
63.3
63.5
63.7
63.9
64.1
V MAG
14
15
16
17
18
66.1
66.3
66.5
66.7
66.9
67.1
67.3
67.5
67.7
67.9
68.1
V MAG
14
15
16
17
18
68.1
68.3
68.5
68.7
68.9
69.1
69.3
69.5
69.7
69.9
70.1
HJD − 2451500

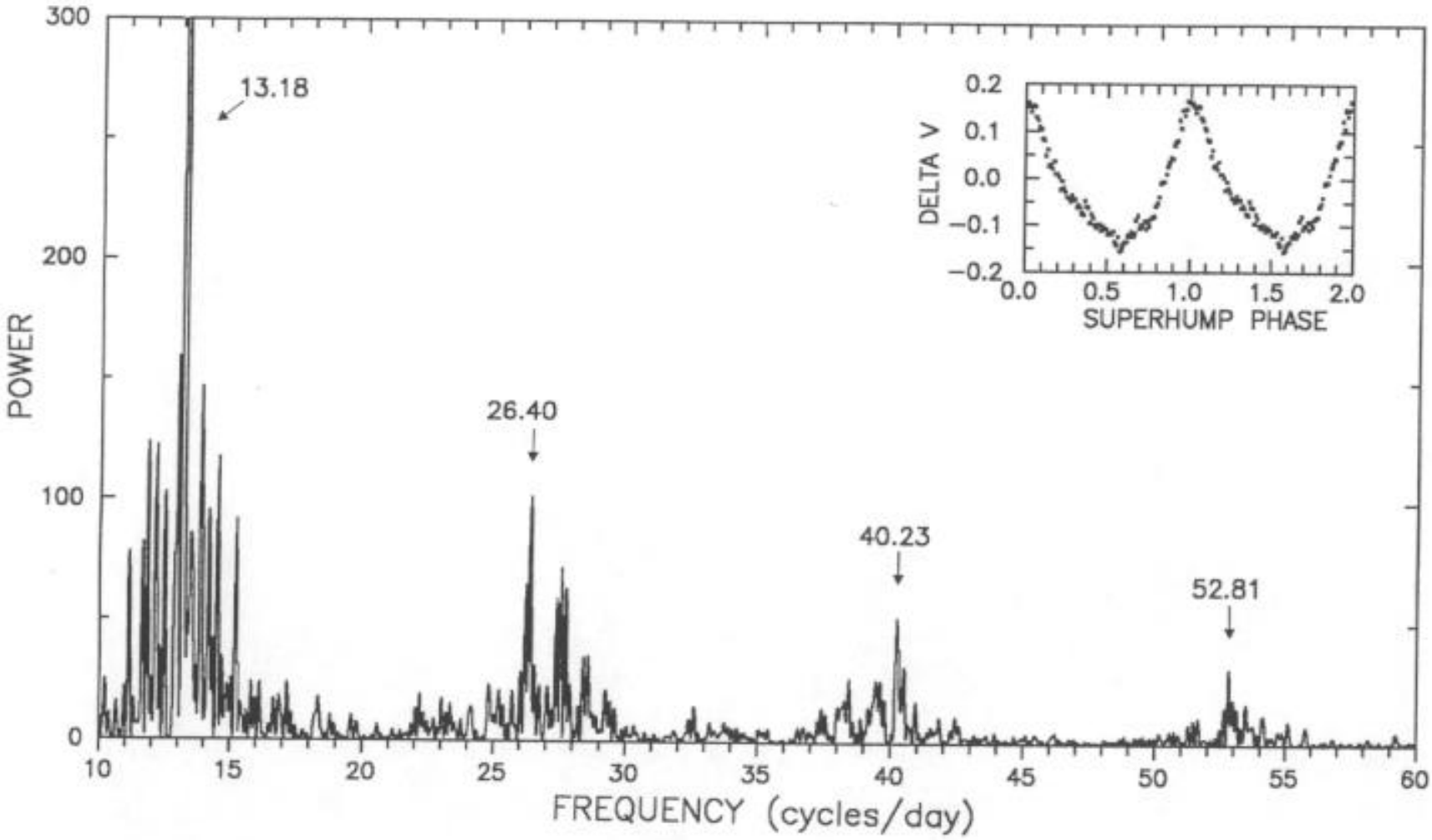
300
200
100
0
POWER
13.18
26.40
40.23
52.81
10
15
20
25
30
35
40
45
50
55
60
FREQUENCY (cycles/day)
0.2
0.1
0.0
−0.1
−0.2
DELTA V
0.0
0.5
1.0
1.5
2.0
SUPERHUMP PHASE

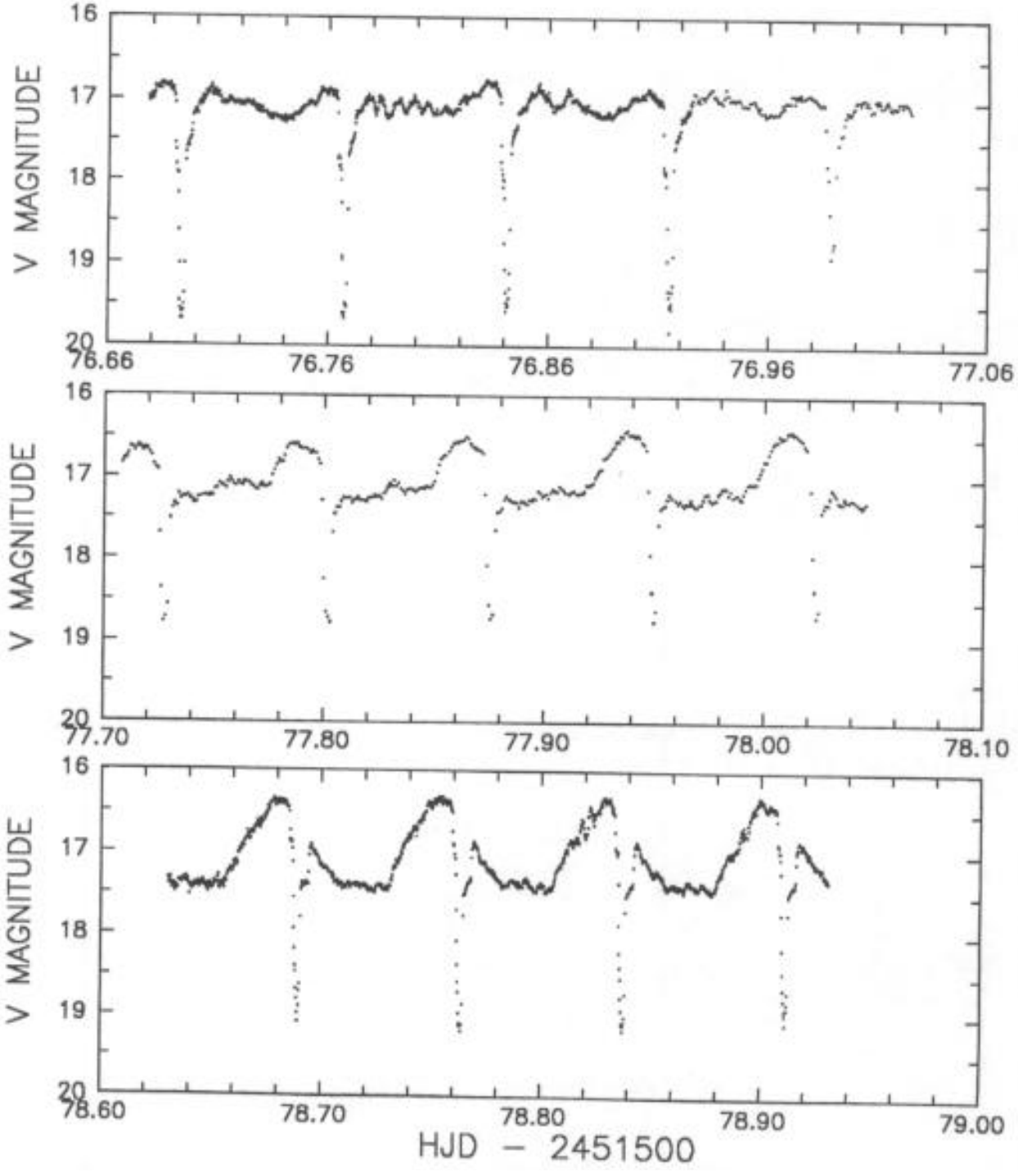
V MAGNITUDE
16
17
18
19
20
76.66
76.76
76.86
76.96
77.06
V MAGNITUDE
16
17
18
19
20
77.70
77.80
77.90
78.00
78.10
V MAGNITUDE
16
17
18
19
20
78.60
78.70
78.80
78.90
79.00
HJD − 2451500

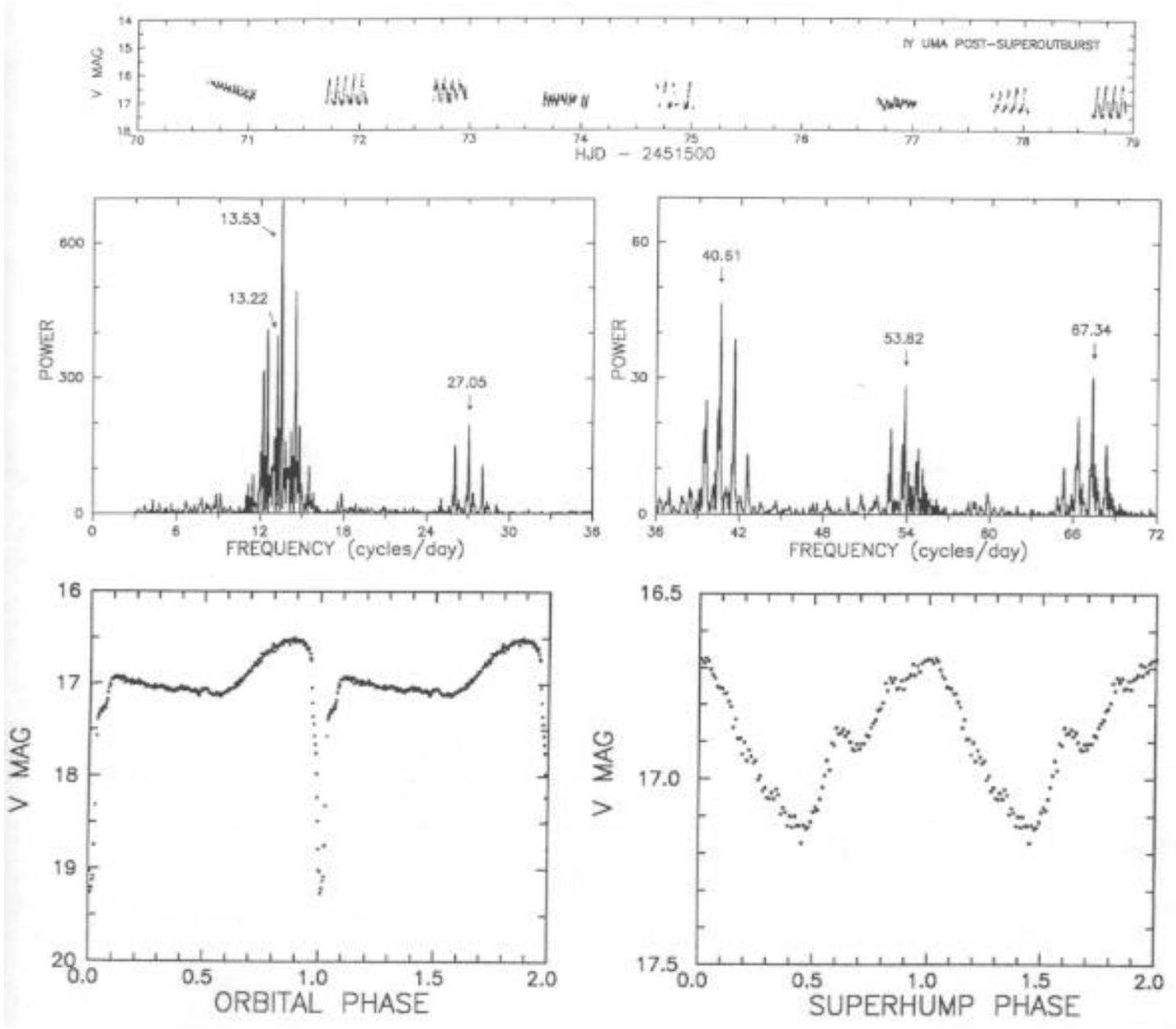
IY UMA POST-SUPEROUTBURST
V MAG
HJD − 2451500
13.53
13.22
27.05
POWER
FREQUENCY (cycles/day)
40.61
53.82
67.34
POWER
FREQUENCY (cycles/day)
V MAG
ORBITAL PHASE
V MAG
SUPERHUMP PHASE

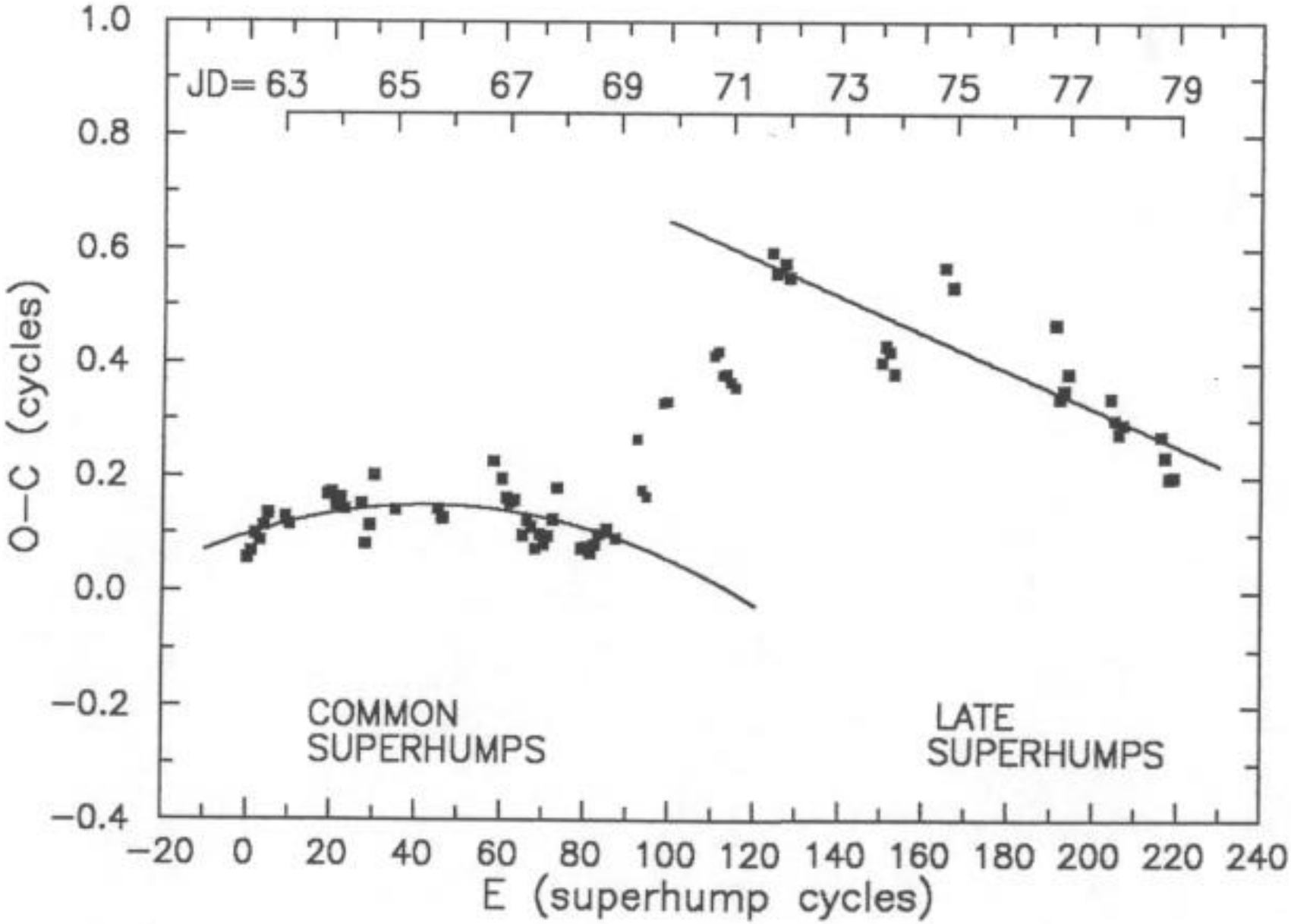
JD= 63
65
67
69
71
73
75
77
79
1.0
0.8
0.6
0.4
0.2
0.0
−0.2
−0.4
O−C (cycles)
COMMON
SUPERHUMPS
LATE
SUPERHUMPS
−20
0
20
40
60
80
100
120
140
160
180
200
220
240
E (superhump cycles)

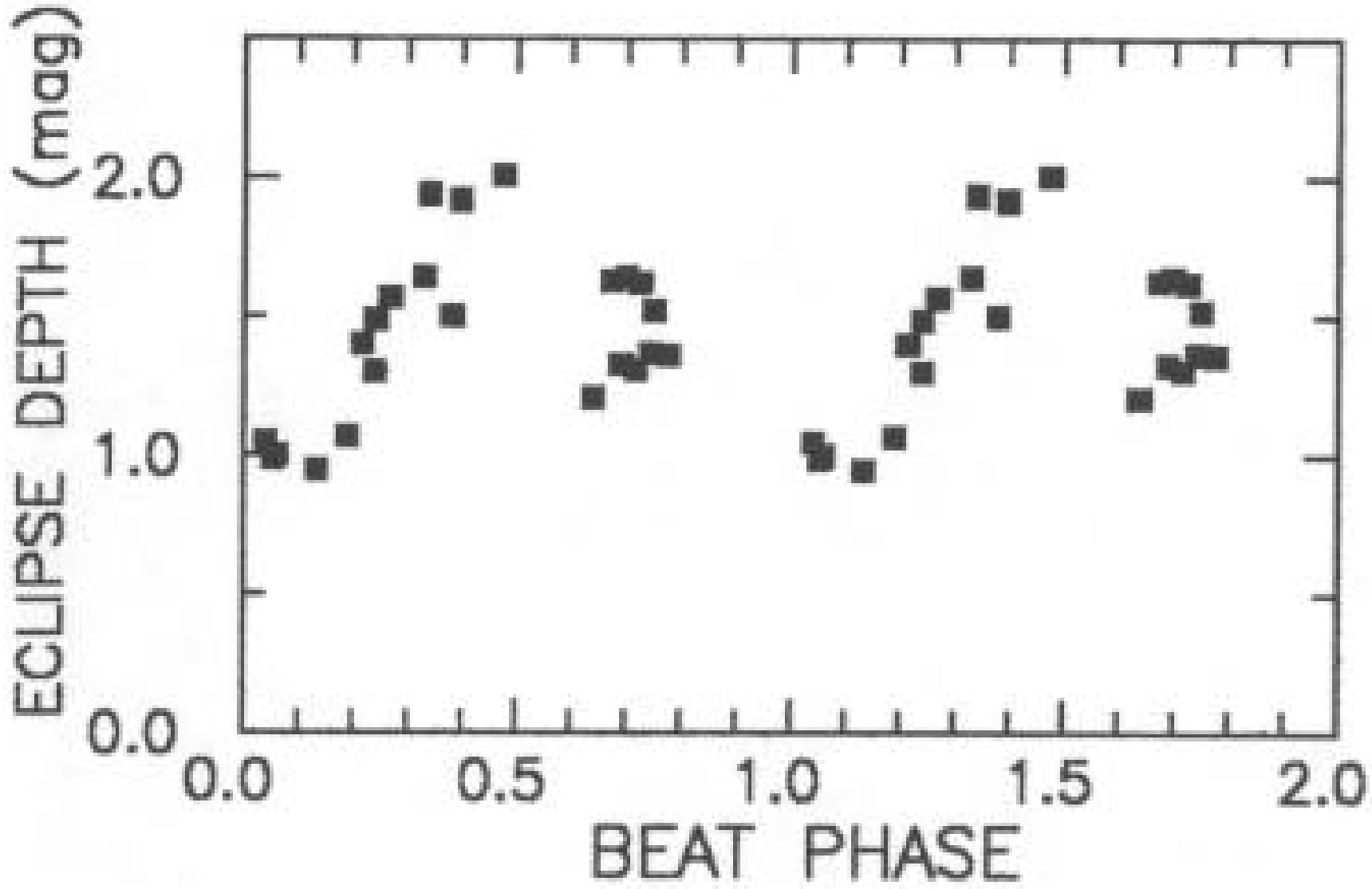
ECLIPSE DEPTH (mag)
2.0
1.0
0.0
0.0
0.5
1.0
1.5
2.0
BEAT PHASE

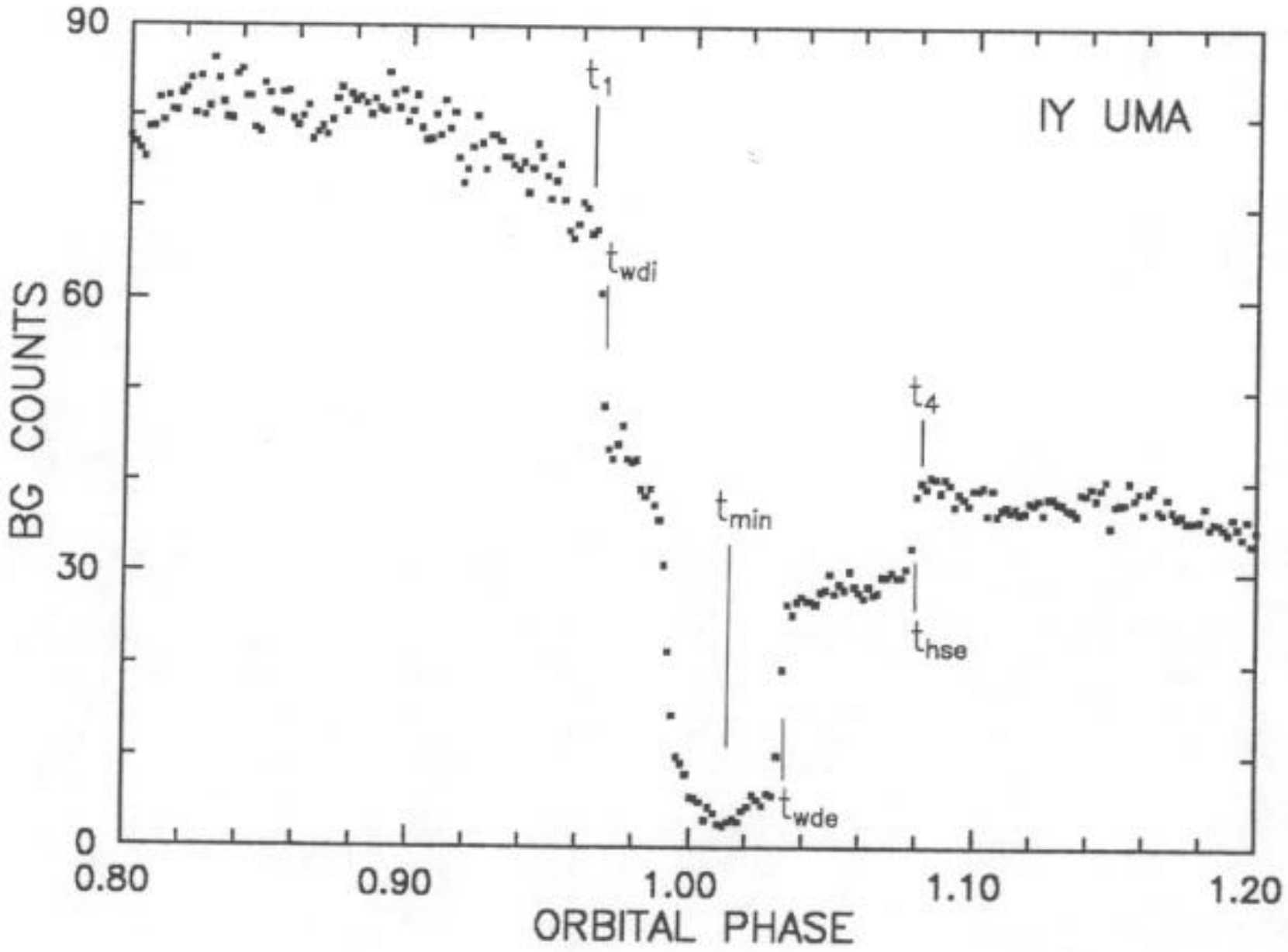
IY UMA
BG COUNTS
ORBITAL PHASE
90
60
30
0
0.80
0.90
1.00
1.10
1.20
$t_1$
$t_{wdi}$
$t_{min}$
$t_{wde}$
$t_4$
$t_{hse}$

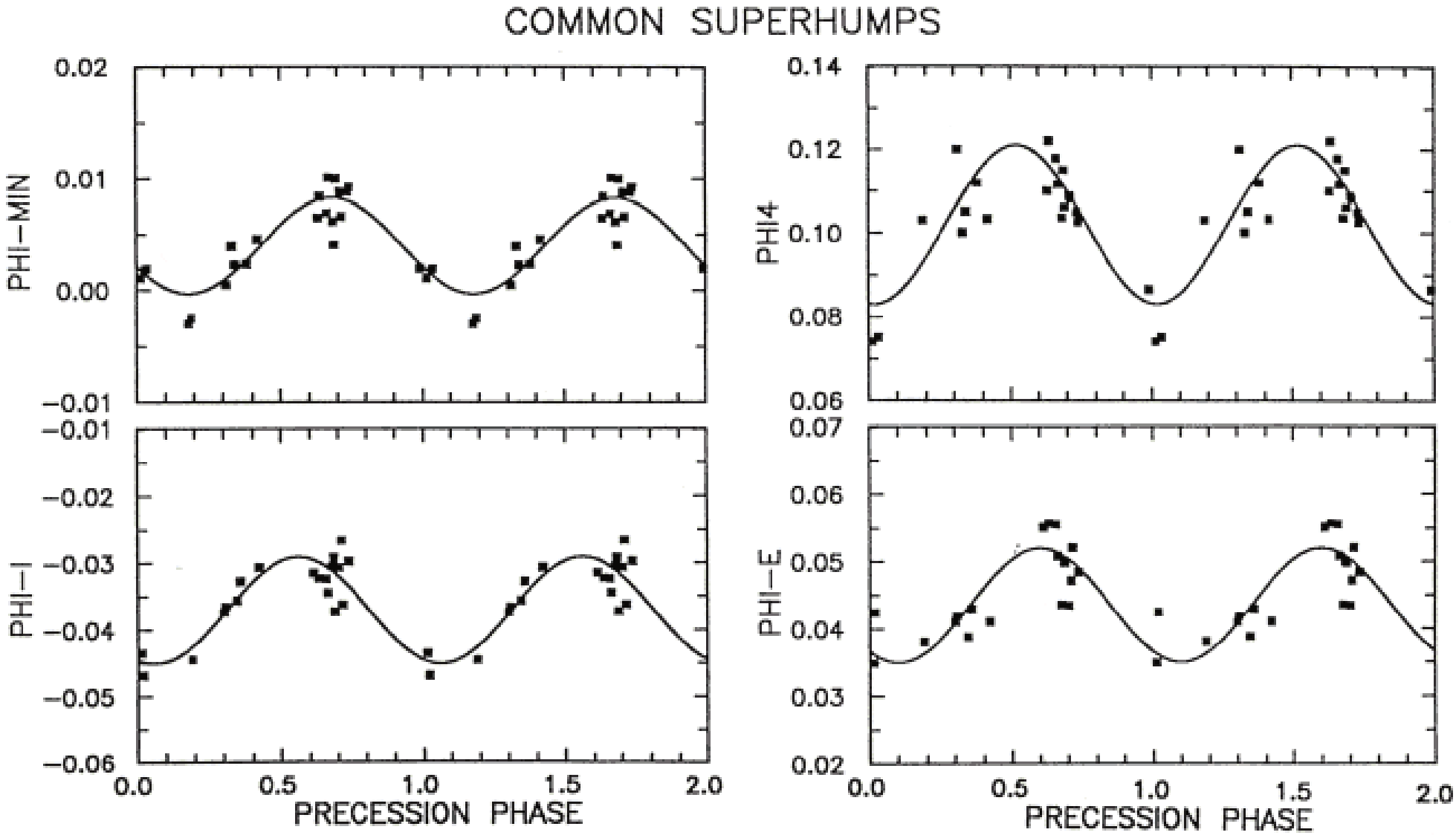
COMMON SUPERHUMPS
PHI−MIN
0.02
0.01
0.00
−0.01
PHI−I
−0.01
−0.02
−0.03
−0.04
−0.05
−0.06
0.0
0.5
1.0
1.5
2.0
PRECESSION PHASE
PHI4
0.14
0.12
0.10
0.08
0.06
PHI−E
0.07
0.06
0.05
0.04
0.03
0.02
0.0
0.5
1.0
1.5
2.0
PRECESSION PHASE

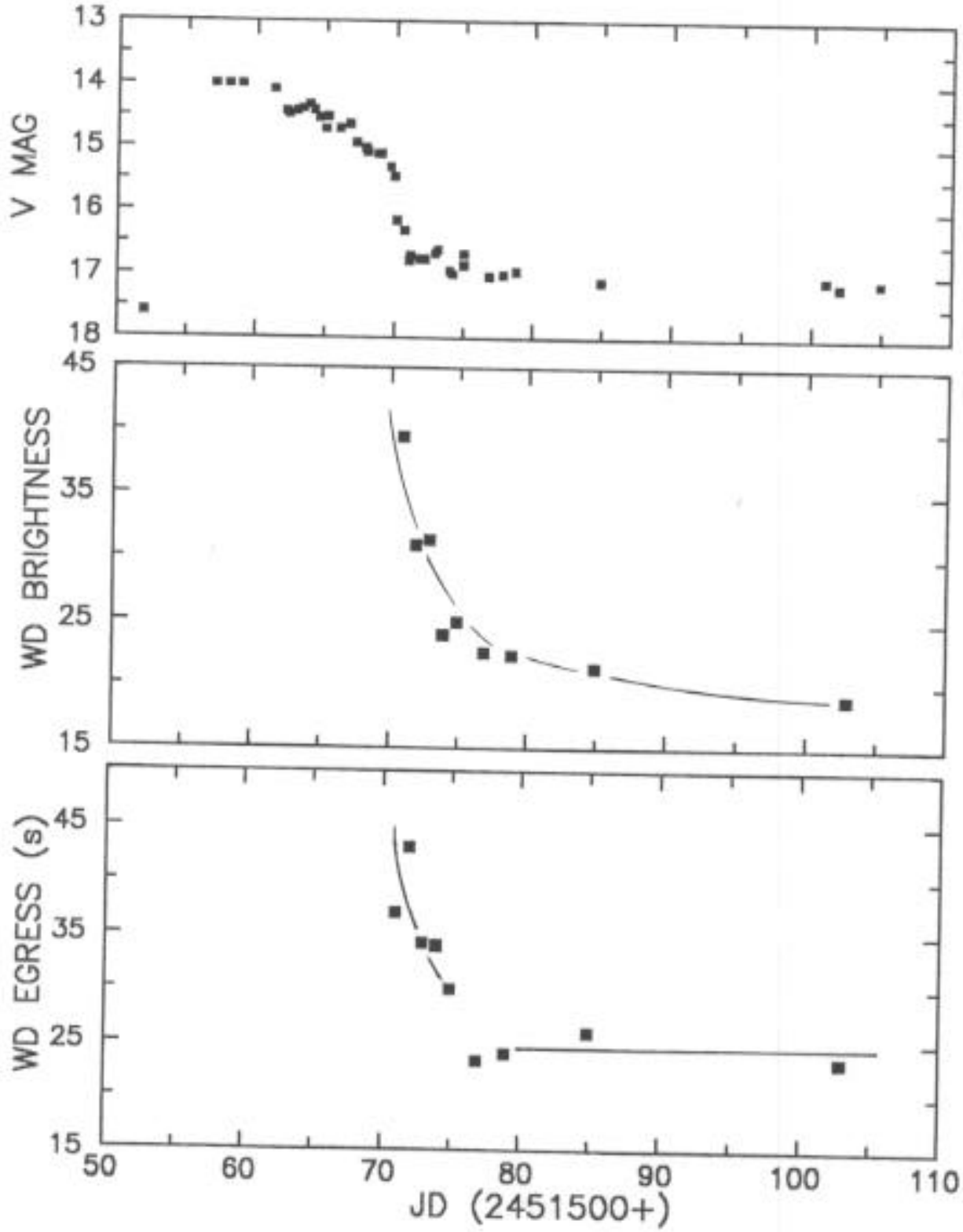
V MAG
13
14
15
16
17
18
WD BRIGHTNESS
45
35
25
15
WD EGRESS (s)
45
35
25
15
50
60
70
80
90
100
110
JD (2451500+)

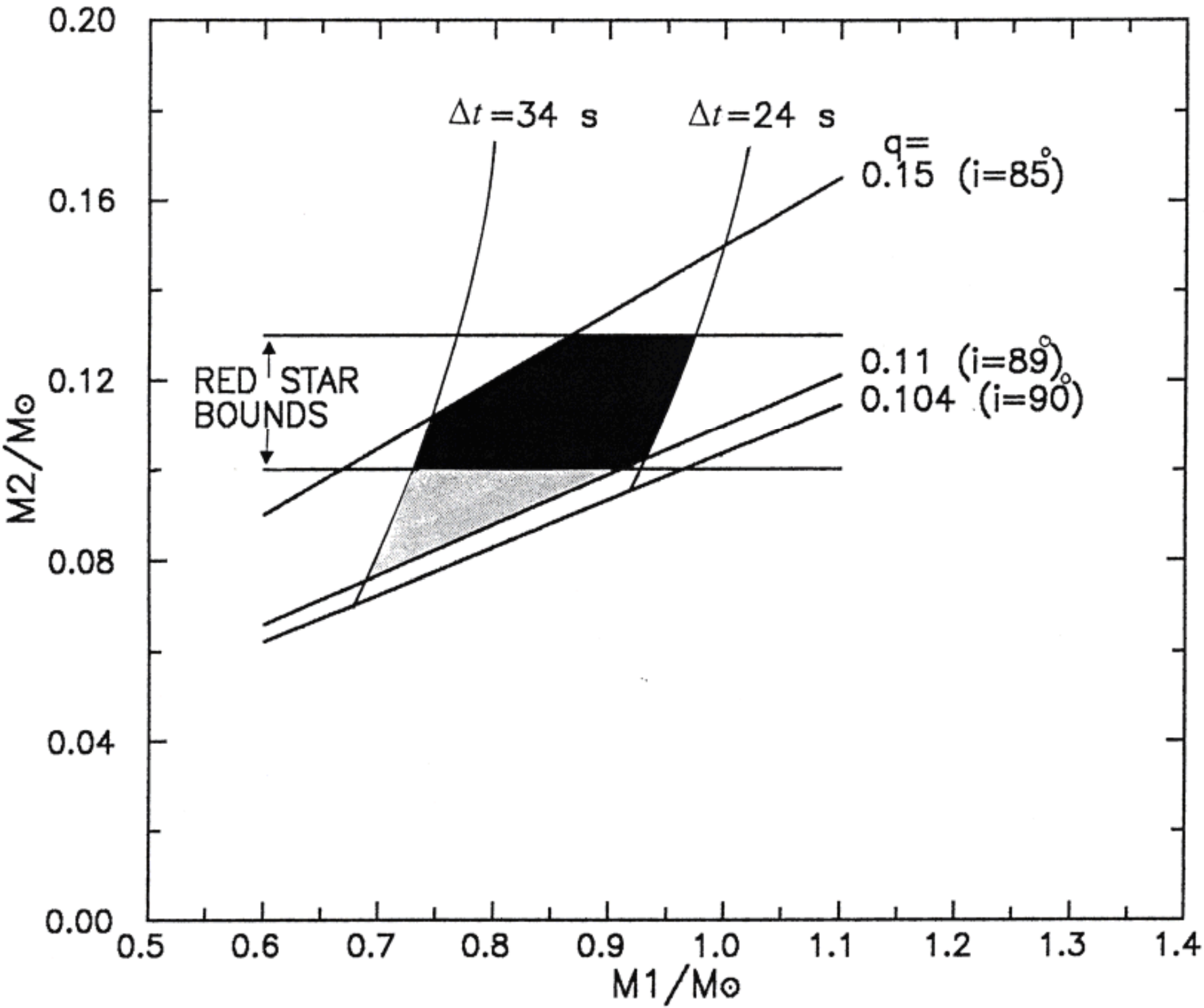
0.20
0.16
0.12
0.08
0.04
0.00
M2/M⊙
0.5
0.6
0.7
0.8
0.9
1.0
1.1
1.2
1.3
1.4
M1/M⊙
Δt =34 s
Δt =24 s
q=
0.15 (i=85°)
0.11 (i=89°)
0.104 (i=90°)
RED STAR
BOUNDS

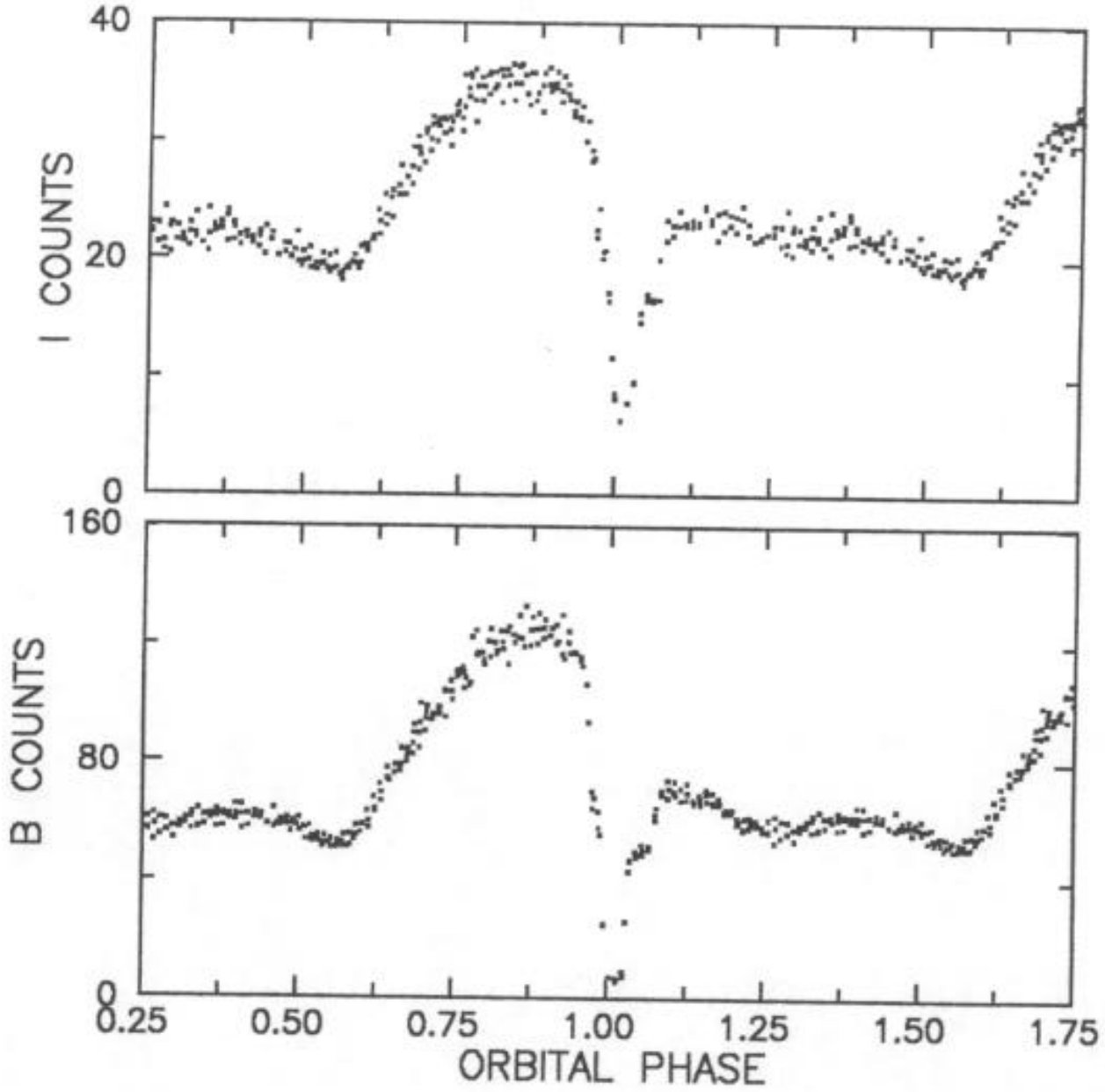
40
20
0
I COUNTS
160
80
0
B COUNTS
0.25
0.50
0.75
1.00
1.25
1.50
1.75
ORBITAL PHASE

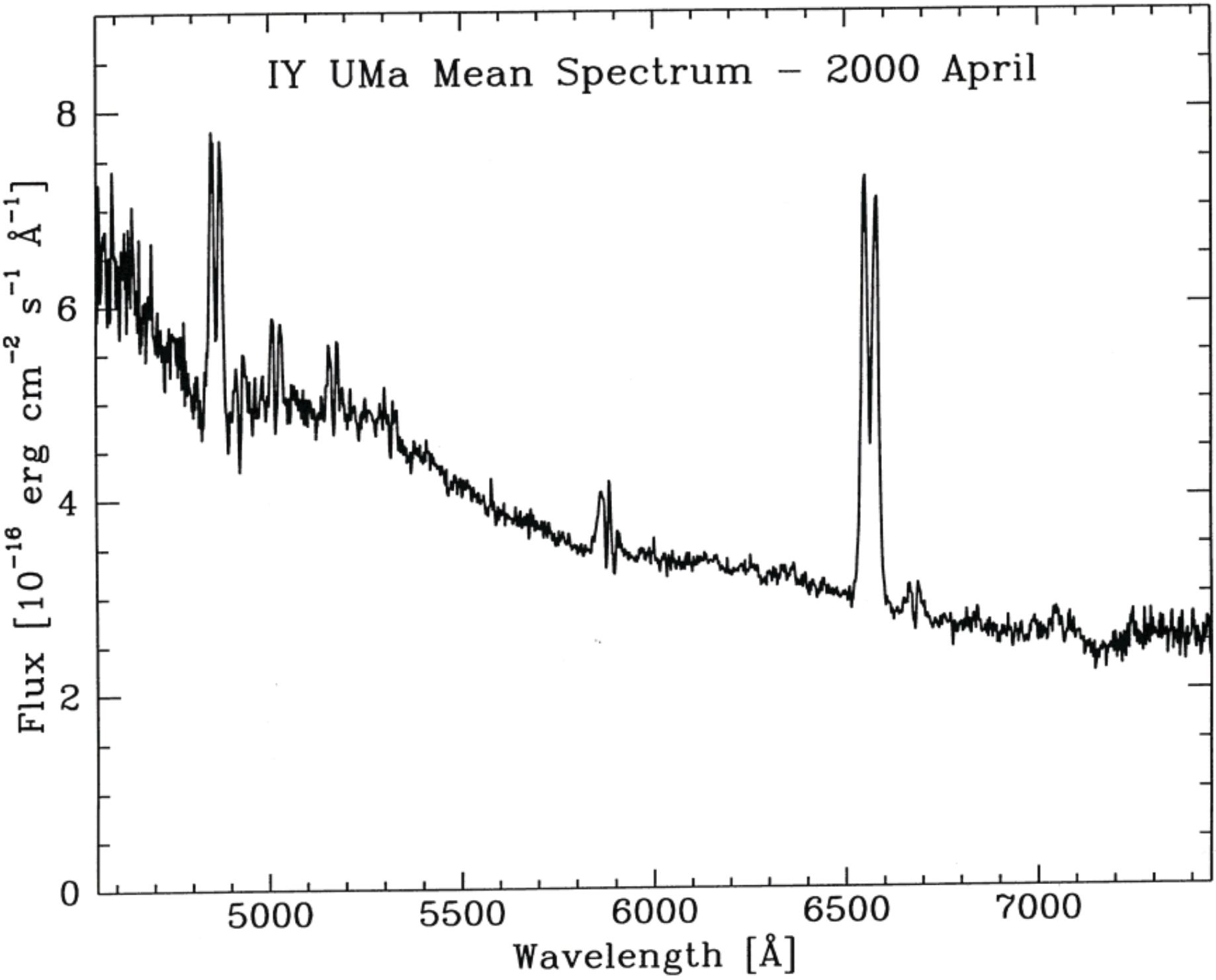
IY UMa Mean Spectrum – 2000 April
Flux [$10^{-16}$ erg cm$^{-2}$ s$^{-1}$ Å$^{-1}$]
0
2
4
6
8
5000
5500
6000
6500
7000
Wavelength [Å]

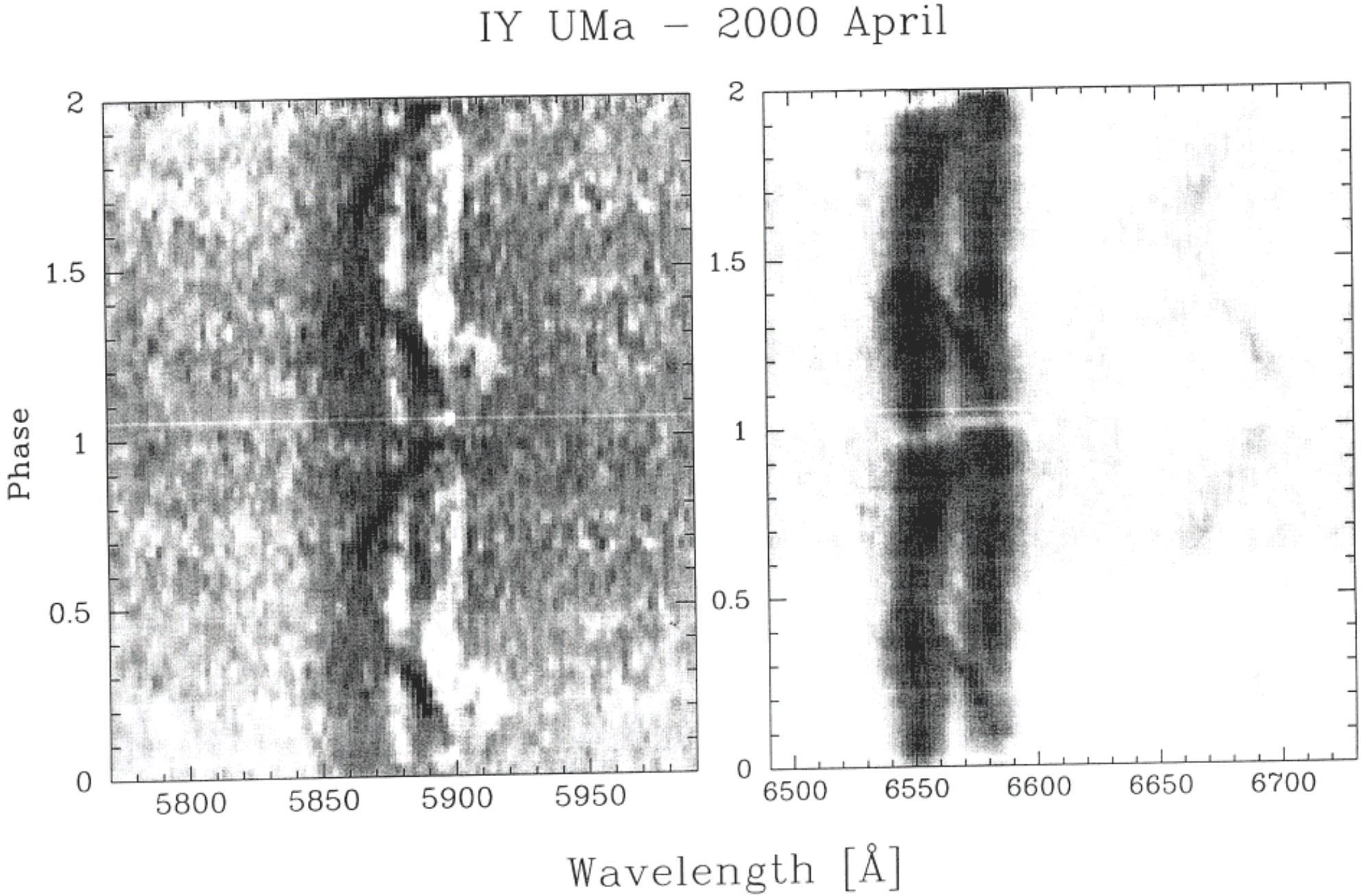
IY UMa – 2000 April
Phase
2
1.5
1
0.5
0
5800
5850
5900
5950
6500
6550
6600
6650
6700
Wavelength [Å]

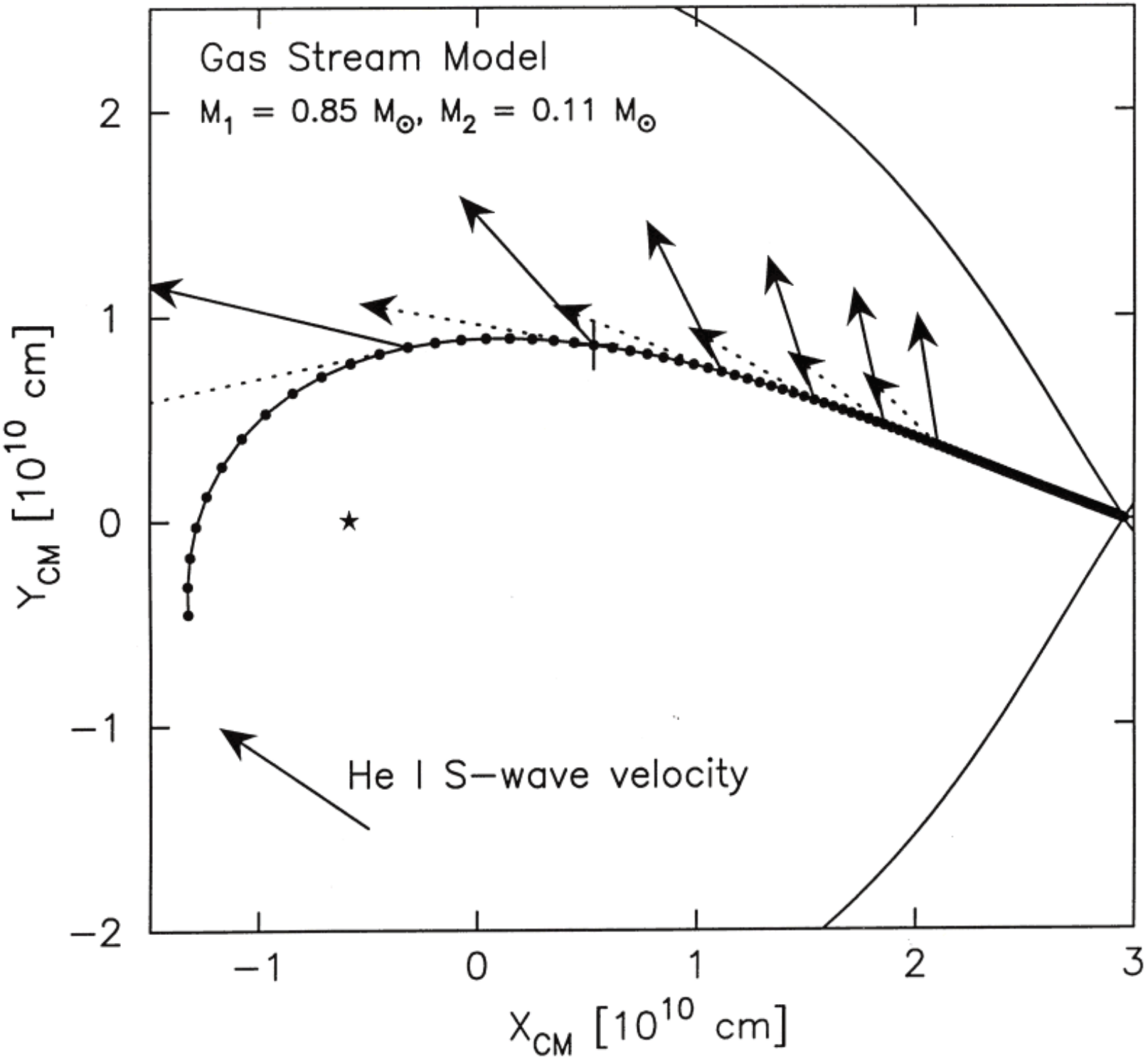
Gas Stream Model
$M_1$ = 0.85 $M_\odot$, $M_2$ = 0.11 $M_\odot$
He I S−wave velocity
$Y_{CM}$ [$10^{10}$ cm]
$X_{CM}$ [$10^{10}$ cm]
2
1
0
−1
−2
−1
0
1
2
3